LIST OF CONTRIBUTORS

TOSHIHIRO KASUGA
Public Relations Center
National Astronomical Observatory of Japan
2-21-1 Osawa Mitaka
Tokyo 181-8588
Japan

Department of Physics
Kyoto Sangyo University
Motoyama, Kamigamo Kita-ku
Kyoto 603-8555
Japan

DAVID JEWITT
Earth, Planetary and Space Sciences / Physics and Astronomy
University of California at Los Angeles
595 Charles Young Drive East Los Angeles
CA 90095-1567
USA

8

Asteroid–Meteoroid Complexes

TOSHIHIRO KASUGA AND DAVID JEWITT

8.1 Introduction

Physical disintegration of asteroids and comets leads to the production of orbit-hugging debris streams. In many cases, the mechanisms underlying disintegration are uncharacterized, or even unknown. Therefore, considerable scientific interest lies in tracing the physical and dynamical properties of the asteroid-meteoroid complexes backwards in time, in order to learn how they form.

Small solar system bodies offer the opportunity to understand the origin and evolution of the planetary system. They include the comets and asteroids, as well as the mostly unseen objects in the much more distant Kuiper belt and Oort cloud reservoirs. Observationally, asteroids and comets are distinguished principally by their optical morphologies, with asteroids appearing as point sources, and comets as diffuse objects with unbound atmospheres (comae), at least when near the Sun. The principal difference between the two is thought to be the volatile content, especially the abundance of water ice. Sublimation of ice in comets drives a gas flux into the adjacent vacuum while drag forces from the expanding gas are exerted on embedded dust and debris particles, expelling them into interplanetary space. Meteoroid streams, consisting of large particles ejected at low speeds and confined to move approximately in the orbit of the parent body, are one result.

When the orbit of the parent body intersects that of the Earth, meteoroids strike the atmosphere and all but the largest are burned up by frictional heating, creating the familiar meteors (Olmsted, 1834). Later, the phenomenon has been realized as ablation by shock wave radiation heating (Bronshten, 1983). The first established comet-meteoroid stream relationships were identified by G. Schiaparelli and E. Weiss in 1866 (see Ceplecha et al., 1998). In the last twenty years, a cometary meteoroid stream theory has been established enabling accurate shower activity prediction of both major (e.g. Leonids, Kondrat'eva et al., 1997; McNaught and Asher, 1999) and minor showers (2004 June Boötids, Vaubaillon et al., 2005). This theory deals with the perturbed motion of streams encountering the Earth after the ejection from relevant parent bodies. This improved theory has provided striking opportunities for meteor shower studies of orbital trajectories, velocities and compositions, resulting in a revolution in meteor science.

Some meteoroid streams seem to be made of debris released from asteroids. The notion that not all stream parents are comets is comparatively old, having been suggested by Whipple (1939a,b, 1940) (see also Olivier, 1925; Hoffmeister, 1937). The Geminid meteoroid stream (GEM/4, from Jopek and Jenniskens, 2011)[1] and asteroid 3200 Phaethon are probably the best-known examples (Whipple, 1983). In such cases, it appears unlikely that ice sublimation drives the expulsion of solid matter, raising the general question of what produces the meteoroid streams? Suggested alternative triggers include thermal stress, rotational instability and collisions (impacts) by secondary bodies (Jewitt, 2012; Jewitt et al., 2015). Any of the above, if sufficiently violent or prolonged, could lead to the production of a debris trail that would, if it crossed Earth's orbit, be classified as a meteoroid stream or an "Asteroid-Meteoroid Complex", comprising streams and several macroscopic, split fragments (Voloshchuk and Kashcheev, 1986; Jones, 1986; Ceplecha et al., 1998).

The dynamics of stream members and their parent objects may differ, and dynamical associations are not always obvious. Direct searches for dynamical similarities employ a distance parameter, $D_{\rm SH}$, which measures the separation in orbital element space by comparing q (perihelion distance), e (eccentricity), i (inclination), Ω (longitude of the ascending node), and ω (argument of perihelion) (Southworth and Hawkins, 1963). A smaller $D_{\rm SH}$ indicates a closer degree of orbital similarity between two bodies, with an empirical cutoff for significance often set at $D_{\rm SH} \lesssim 0.10$–0.20 (Williams et al., 2019, Section 9.2.2). The statistical significance of proposed parent-shower associations has been coupled with $D_{\rm SH}$ (Wiegert and Brown, 2004; Ye et al., 2016). Recent models assess the long-term dynamical stability for high-i and -e asteroids. Ohtsuka et al. (2006, 2008a) find the Phaethon-Geminid Complex (PGC) and the Icarus complex together using as criteria the C_1 (Moiseev, 1945) and C_2 (Lidov, 1962) integrals. These are secular orbital variations expressed by

$$C_1 = (1-e^2)\cos^2(i) \quad (8.1)$$

$$C_2 = e^2\,(0.4 - \sin^2(i)\sin^2(\omega)). \quad (8.2)$$

So-called time-lag theory is utilized to demonstrate long-term orbital evolution of complex members. When a stream-complex is formed, the orbital energies ($\propto a^{-1}$, where a is the semimajor axis) of ejected fragments are expected to be slightly different from the energy of the precursor. The mo-

[1] IAU Meteor Data Center, Nomenclature

tions of the released objects are either accelerated or decelerated relative to the precursor under gravitational perturbations (possibly including non-gravitational perturbations), effectively causing a time lag, Δt, in the orbital evolution to arise. Both C_1 and C_2 are approximately invariant during dynamical evolution, distinguishing the complex members. The PGC members (Phaethon, 2005 UD, 1999 YC), for example, dynamically follow the Lidov-Kozai mechanism based on secularly perturbed motion of the asteroids (Kozai, 1962).

Most known parent bodies are near-Earth Objects (NEOs), including both asteroids and comets. The comets include various sub-types: Jupiter family comets (JFCs), Halley type comets (HTCs) and Encke-type comets (Ye, 2018) (Table 8.1). A classification of parents and their associated streams has been proposed based on their inferred evolutionary stages (Babadzhanov and Obrubov, 1987, 1991, 1992a,b). Some streams originating from asteroids (e.g. Phaethon), or from comets (e.g. 96P, 2P) are the most evolved. For example, the Geminids, Quadrantids (QUA/10) and Taurid Complex (TAU/247) show stable secular variation of the orbital elements under the mean motion resonance with Jupiter and the Kozai resonance, producing annual meteor showers. On the other hand, young streams are usually from JFCs and HTCs. JFCs orbits, in particular, are chaotically scattered by frequent close encounters with Jupiter, tending to produce irregular streams, e.g. Phoenicids (PHO/254). HTCs orbit with widespread inclinations, including retrograde orbits that are absent in the JFCs, and may also generate regular showers, e.g. Leonids (LEO/13) and Perseids (PER/7).

Non-gravitational force effects can be important in the evolution of stream complexes but are difficult to model, since they depend on many unknowns such as the size, rotation, and thermal properties of the small bodies involved. In the last decade, video- and radar- based surveys of meteors have also been used to trace the trajectories back to potential parent NEOs, and so to find new stream complexes (e.g. Brown et al., 2008a,b, 2010; Musci et al., 2012; Jenniskens, 2008a; Weryk and Brown, 2012; Rudawska et al., 2015; Jenniskens et al., 2016a,b; Jenniskens and Nénon, 2016; Ye et al., 2016) (Reviewed in Jenniskens, 2017).

Meteor spectroscopy provides some additional constraints on the composition of meteoroids (Millman and McKinley, 1963; Millman, 1980). Spectroscopy is typically capable of obtaining useful data for meteors having optical absolute magnitudes +3 to +4 or brighter, corresponding to meteoroid sizes $\gtrsim$ 1 mm (Lindblad, 1987; Ceplecha et al., 1998; Borovička et al., 2010). Meteor spectra consist primarily of atomic emission lines and some molecular bands in the visible to near-infrared wavelengths. The commonly identified neutral atoms are Mg I, Fe I, Ca I, and Na I, while the singly ionized atomic emissions of Ca II and Mg II also appear in some fast-moving meteors (e.g. Leonids with geocentric velocity V_g ∼72 km s^{-1} impact much more quickly than the Geminids, with $V_g \sim 35\,\mathrm{km\,s^{-1}}$). The abundances, the excitation temperatures and the electron densities can be deduced for each spectrum, assuming the Boltzmann distribution for electron energies, but the measurements are difficult, and the resulting elemental abundances and/or intensity ratios (e.g. Nagasawa, 1978; Borovicka, 1993; Kasuga et al., 2005b; Borovička et al., 2005) are scattered (summarized in Ceplecha et al., 1998; Kasuga et al., 2006). Generally, most meteors are found to have solar abundance within factors of ∼3–4. Some elements are noticeably underabundant, probably affected by incomplete evaporation (Trigo-Rodríguez et al., 2003; Borovicka et al., 1999; Kasuga et al., 2005b). In particular, sodium (Na) is a relatively abundant and moderately volatile element that is easily volatilized. As a result, the abundance of Na in meteors is a good indicator of thermal evolution of meteoroids. Heating either during their residence in interplanetary space or within the parent bodies themselves can lead to a sodium depletion.

In this chapter, we give a brief summary of observational results on parents and their associated showers. We discuss the properties of specific complexes, and tabulate their dynamical and physical properties (Tables 8.1, 8.2). We focus on the main meteoroid streams for which the properties and associations seem the most secure. Numerous additional streams and their less certain associations are discussed in the literature reviewed by (Jenniskens, 2006, 2008b; Borovička, 2007; Ye, 2018; Vaubaillon et al., 2019, Section 7.5).

8.2 General Properties

To date, twelve objects in the six asteroid-meteoroid complexes have been studied in detail. Figure 8.1 represents their distributions in the semimajor axis versus eccentricity plane, while Figure 8.2 shows semimajor axis versus inclination (Table 8.1 summarizes the orbital properties).

Traditionally, the Tisserand parameter with respect to Jupiter, T_J, is used to characterize the dynamics of small bodies (Kresak, 1982; Kosai, 1992). It is defined by

$$T_J = \frac{a_J}{a} + 2\left[(1-e^2)\frac{a}{a_J}\right]^{1/2}\cos(i) \qquad (8.3)$$

where a, e and i are the semimajor axis, eccentricity and inclination of the orbit and $a_J = 5.2$ AU is the semimajor axis of the orbit of Jupiter. This parameter, which is conserved in the circular, restricted 3-body problem, provides a measure of the close-approach speed to Jupiter. Jupiter itself has $T_J = 3$. Main belt asteroids have $a < a_J$ and $T_J > 3$ while dynamical comets from the Kuiper belt have $2 \leq T_J < 3$ and comets from the Oort cloud have $T_J < 2$. In principle, the asteroids and comets can also be distinguished compositionally. The main belt asteroids are generally rocky, non-icy objects which probably formed inside snow-line in the protoplanetary disk, while comets contain a larger ice fraction and formed beyond it. In practice, it is difficult or impossible to measure the compositions of most small bodies in the solar system, so that composition is not often a useful diagnostic.

The use of T_J as a discriminant breaks down near $T_J \simeq 3$, since the definition assumes that Jupiter's orbit is a circle,

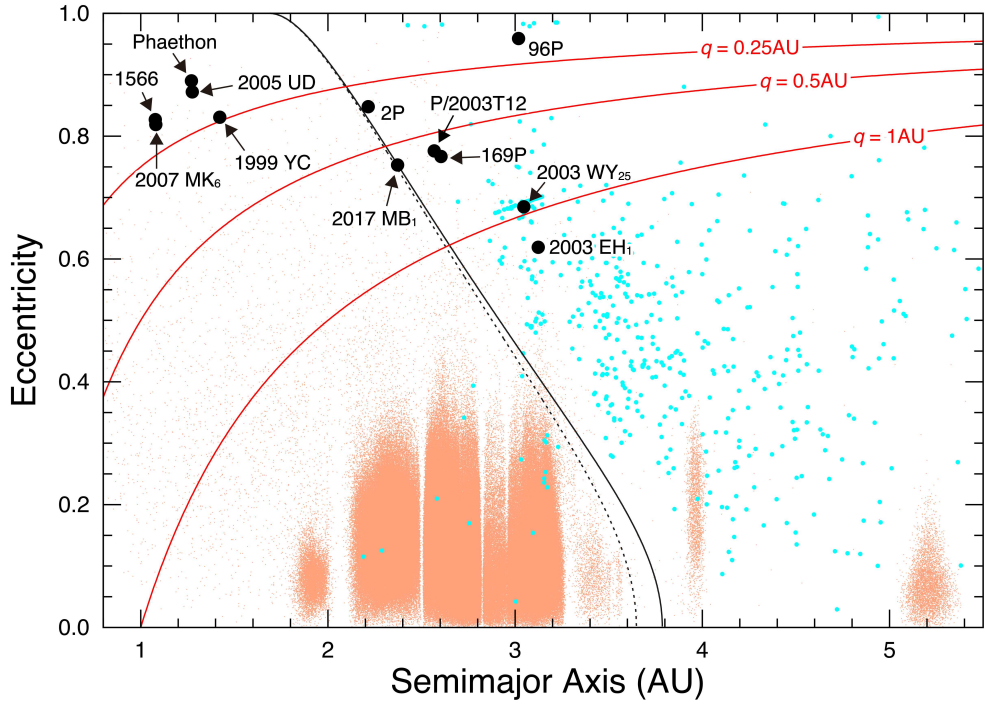

Figure 8.1 Distribution of the parent bodies (black circles) in the semimajor axis vs. orbital eccentricity plane (cf. Table 8.1). The distributions of asteroids (brown dots) and comets (light-blue dots) are shown for reference. The lines for $T_J = 3.08$ with i=0° (solid curve) and with i=9° (dotted curve) broadly separate asteroids and comets. Perihelion distances $q = 0.25$, 0.5 and 1 AU are shown as red curves.

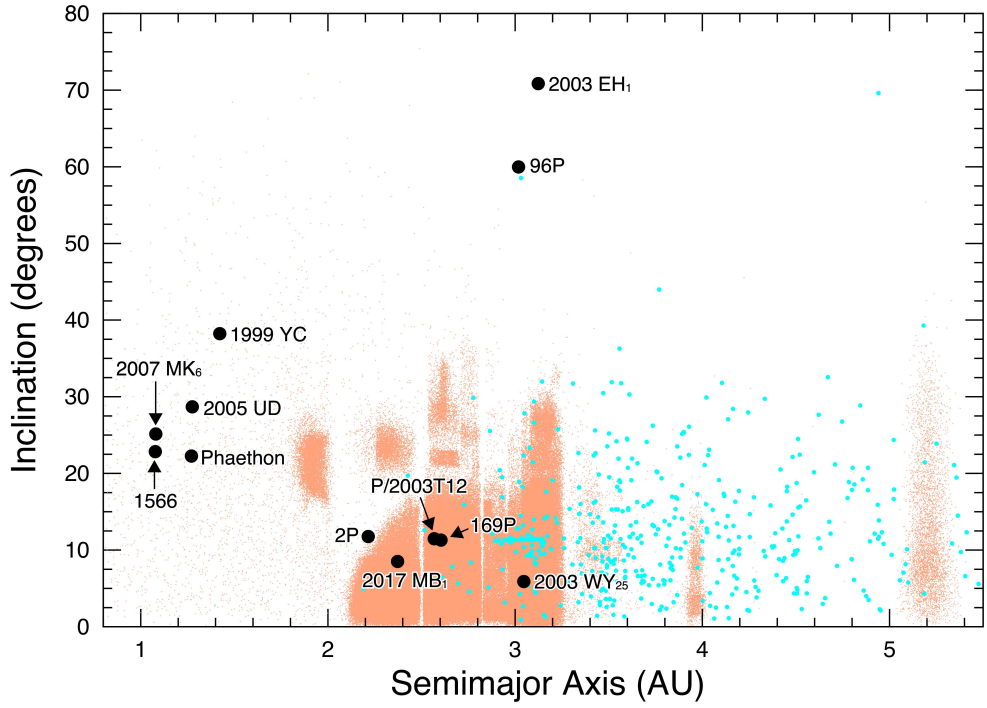

Figure 8.2 Same as Figure 8.1 but semimajor axis vs. inclination.

Table 8.1. *Orbital Properties*

Complex	Object	a[a]	e[b]	i[c]	q[d]	ω[e]	Ω[f]	Q[g]	$P_{\rm orb}$[h]	C_1[i]	C_2[i]	$T_{\rm J}$[j]
Geminids	Phaethon	1.271	0.890	22.253	0.140	322.174	265.231	2.402	1.43	0.178	0.274	4.509
	2005 UD	1.275	0.872	28.682	0.163	207.573	19.746	2.387	1.44	0.184	0.267	4.504
	1999 YC	1.422	0.831	38.226	0.241	156.395	64.791	2.603	1.70	0.191	0.234	4.114
Quadrantids	2003 EH_1	3.123	0.619	70.838	1.191	171.361	282.979	5.056	5.52	0.066	0.146	2.065
	96P/Machholz 1	3.018	0.959	59.975	0.125	14.622	94.548	5.911	5.24	0.020	0.324	1.939
Capricornids	169P/NEAT	2.604	0.767	11.304	0.607	217.977	176.219	4.602	4.20	0.396	0.227	2.887
	P/2003 T12	2.568	0.776	11.475	0.575	217.669	176.465	4.561	4.12	0.382	0.232	2.894
	2017 MB_1	2.372	0.753	8.508	0.586	264.628	126.974	4.158	3.65	0.424	0.215	3.071
Taurids	2P/Encke	2.215	0.848	11.781	0.336	186.542	334.569	4.094	3.30	0.269	0.287	3.025
Taurids-Perseids	1566 Icarus	1.078	0.827	22.852	0.187	31.297	88.082	1.969	1.12	0.268	0.246	5.296
	2007 MK_6	1.081	0.819	25.138	0.196	25.466	92.887	1.966	1.12	0.270	0.246	5.284
Phoenicids	2003 WY_{25}	3.046	0.685	5.9000	0.961	9.839	68.931	5.132	5.32	0.525	0.188	2.816

Notes: Orbital data are obtained from NASA JPL HORIZONS (https://ssd.jpl.nasa.gov/horizons.cgi)
[a] Semimajor axis (AU)
[b] Eccentricity
[c] Inclination (degrees)
[d] Perihelion distance (AU)
[e] Argument of perihelion (degrees)
[f] Longitude of ascending node (degrees)
[g] Aphelion distance (AU)
[h] Orbital period (yr)
[i] Dynamical invariants: $C_1 = (1 - e^2)\cos^2(i)$, $C_2 = e^2\,(0.4 - \sin^2(i)\sin^2(\omega))$
[j] Tisserand parameter with respect to Jupiter (asteroids with $T_J > 3.08$, comets with $T_J < 3.08$; $a < a_J(5.2\,{\rm AU})$)

the gravity of other planets is neglected, and so on. Accordingly, a functional definition for the boundary employed here is $T_J \simeq 3.08$ (Jewitt et al., 2015), shown in Figure 8.1, where the solid curve represents T_J computed assuming $i = 0^\circ$, while the dotted curve is the same but with $i = 9^\circ$ (equal to the average inclination of 516,633 numbered objects in the JPL Horizons database). They are very similar, indicating the definition broadly works independently of i. This avoids chaotic cases caused by deviation of the real solar system from the circular, restricted 3-body approximation. Also, comet 2P/Encke with $T_J \sim 3.03$ and the quasi-Hilda comets with $T_J \sim 2.9 - 3.04$ are appropriately classified with this criterion.

As seen in Figure 8.1, all of the parent bodies have $e \gtrsim 0.6$. Seven objects fall on the right side of the boundary with $T_J < 3.08$, corresponding to the region of comets. Mass-loss activity has been directly detected in most of them, although 2003 EH_1 and 2017 MB_1 have yet to show evidence for current activity. Objects on the left side of the diagram are classified in the region of the asteroids, with $T_J > 3.08$. In these objects, a range of physical processes appear to drive the mass loss. They have small $q \lesssim 0.25$ AU and are categorized as near-Sun objects (see Figure 8.1). Recurrent activity of Phaethon at perihelion, including the formation of a tail, has been reported.

In Figure 8.2, 2003 EH_1 and 96P show remarkably high-i $\gtrsim 60^\circ$. Five objects with $a = 1.0 \sim 1.4$ AU have moderate i of $20^\circ \sim 40^\circ$. Another five objects at $a = 2.2 \sim 3.1$ AU have low-i, compatible with those of most main belt asteroids.

8.3 Known Asteroid-Meteoroid Complexes

The physical properties of the main asteroid-meteoroid complexes are listed in Table 8.2, and we review them focusing on the observational evidence.

8.3.1 Geminids – (3200) Phaethon

The Geminid meteor shower is one of the most active annual showers (Whipple, 1939b; Spurný, 1993). The shower currently has zenithal hourly rate (ZHR), the number of meteors visible per hour under a clear-dark sky ($\lesssim$ limiting magnitude +6.5), of ~ 120 and is expected to continue to increase to a peak ZHR ~ 190 in 2050 as the Earth moves deeper into the stream core (Jones and Hawkes, 1986; Jenniskens, 2006). The Geminids are dynamically associated with the near-Earth asteroid (3200) Phaethon (1983 TB) (Whipple, 1983) (Figure 8.3). A notable orbital feature of both is the small perihelion distance, $q \sim 0.14$ AU, raising the possibility of strong thermal processing of the surface. Indeed, the peak temperature at perihelion is $\sim$1000 K (Ohtsuka et al., 2009).

Spectroscopy of Geminid meteors shows an extreme diversity in Na content, from strong depletion of Na abundance in some to sun-like values in others. Kasuga et al. (2005a) found a huge depletion in the Na/Mg abundance ratio of a Geminid meteor, with a value an order of magnitude smaller than the solar abundance ratio (Anders and Grevesse, 1989; Lodders, 2003). Line intensity ratios of Na I, Mg I, and Fe I emissions of the Geminids also show a wide range of Na line strengths, from undetectable to intense (Borovička et al.,

Table 8.2. *Physical Properties*

Complex	Object	D_e[a]	p_v[b]	$P_{\rm rot}$[c]	$B-V$[d]	$V-R$[d]	$R-I$[d]	a/b[e]
Geminids	Phaethon[1]	5–6	0.09–0.13	3.604	0.59±0.01	0.35±0.01	0.32±0.01	∼1.45
	2005 UD[2]	1.3±0.1	0.11[f]	5.249	0.66±0.03	0.35±0.02	0.33±0.02	1.45±0.06
	1999 YC[3]	1.7±0.2[g]	0.09±0.03[g]	4.495	0.71±0.04	0.36±0.03	-	1.89±0.09
Quadrantids	2003 EH_1[4]	4.0±0.3	0.04[f]	12.650	0.69±0.01	0.39±0.01	0.38±0.01	1.50±0.01
	96P/Machholz 1[5]	6.4	0.04[f]	6.38	-	0.40±0.03	-	1.4 ≤
Capricornids	169P/NEAT[6]	4.6±0.6	0.03±0.01	8.410	0.73±0.02	0.43±0.02	0.44±0.04	1.31±0.03
	P/2003 T12	-	-	-	-	-	-	-
	2017 MB_1[7]	0.52	-	6.69	-	-	-	∼1.2
Taurids	2P/Encke[8]	4.8±0.4	0.05±0.02	11	0.73±0.06	0.39±0.06	-	1.44±0.06
Taurids-Perseids	1566 Icarus[9]	1.0–1.3	0.30–0.50[h]	2.273	0.76±0.02	0.41±0.02	0.28±0.02	1.2–1.4
	2007 MK_6	0.18[i]	0.40[f]	-	-	-	-	-
Phoenicids	2003 WY_{25}[10]	≤0.32	0.04[f]	-	-	-	-	-

Notes:
[a] Effective diameter (km)
[b] Geometric albedo
[c] Rotational period (hr)
[d] Color index. Solar colors are $B-V$=0.64±0.02, $V-R$=0.35±0.01 and $R-I$=0.33±0.01 (Holmberg et al., 2006).
[e] Axis ratio
[f] Assumed value
[g] D_e=1.4±0.1 with the assumed p_v=0.11 (Kasuga and Jewitt, 2008).
[h] Extremely high $p_v > 0.7$ is given $D_e < 0.8$ km (Mahapatra et al., 1999; Harris and Lagerros, 2002).
[i] Estimated from the absolute magnitude H=20.3 (MPO386777) with the assumed p_v=0.40.
[1] Green et al. (1985); Tedesco et al. (2004); Dundon (2005); Ansdell et al. (2014); Hanuš et al. (2016); Taylor et al. (2018) [2] Jewitt and Hsieh (2006); Kinoshita et al. (2007) [3] Kasuga and Jewitt (2008); Mainzer et al. (2011); Warner (2017)[4] Kasuga and Jewitt (2015) [5] Licandro et al. (2000); Meech et al. (2004); Lamy et al. (2004) [6] Kasuga et al. (2010); Weissman et al. (2004); A'Hearn et al. (2005); DeMeo and Binzel (2008) [7] Warner (2018) [8] Kokotanekova et al. (2017); Lamy et al. (2004); Campins and Fernández (2002); Lowry and Weissman (2007b); Fernández et al. (2000) [9] Gehrels et al. (1970); Veeder et al. (1989); Chapman et al. (1994); Nugent et al. (2015); Miner and Young (1969); Harris (1998); Angelis (1995); Dundon (2005) [10] Jewitt (2006)

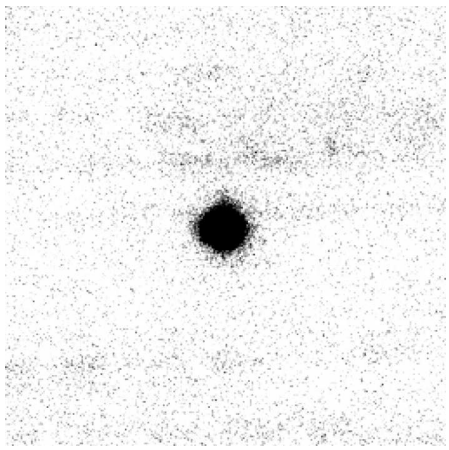

Figure 8.3 Composite R-band image of Phaethon taken at the University of Hawai'i 2.2-m telescope (UH2.2) on UT 2003 December 19. The full image width is 1' and this is a 3600 s equivalent integration, with Phaethon at heliocentric distance R = 1.60 AU, geocentric distance Δ = 1.39 AU, and phase angle α = 0.3°. The image shows no evidence of mass-loss activity. From Hsieh and Jewitt (2005).

2005). Studies of Geminid meteor spectra, reported since the 1950s (e.g. Millman, 1955; Russell et al., 1956; Harvey, 1973; Borovička, 2001; Trigo-Rodríguez et al., 2003, 2004), mostly fit this pattern.

As a summary for Na in the Geminids in the last decade, Kasuga et al. (2006) investigated perihelion dependent thermal effects on meteoroid streams. The effect is supposed to alter the metal abundances from their intrinsic values in their parents, especially for temperature-sensitive elements: a good example is Na in alkaline silicate. As a result, meteoroid streams with $q \lesssim 0.1$ AU should be depleted in Na by thermal desorption, because the corresponding meteoroid temperature (characterized as blackbody) exceeds the sublimation temperature of alkaline silicates ($\sim$ 900 K for sodalite: $Na_4(AlSiO_4)_3Cl$). For this reason, the Na loss in Geminids ($q \sim 0.14$ AU) is most likely to be caused by thermal processes on Phaethon itself (see section 8.6.1).

The parent body Phaethon (diameter 5 – 6 km, from Tedesco et al., 2004; Taylor et al., 2018) has an optically blue (so-called "B-type") reflection spectrum that distinguishes it from most other asteroids and from the nuclei of comets. Specifically, only $\sim$ 1 in 23 asteroids is of B-spectral type and most cometary nuclei are slightly reddish, like the C-type asteroids or the (redder) D-type Jovian Trojans.

A dynamical pathway to another B-type, the large main-belt asteroid (2) Pallas, has been reported with $\sim$ 2% prob-

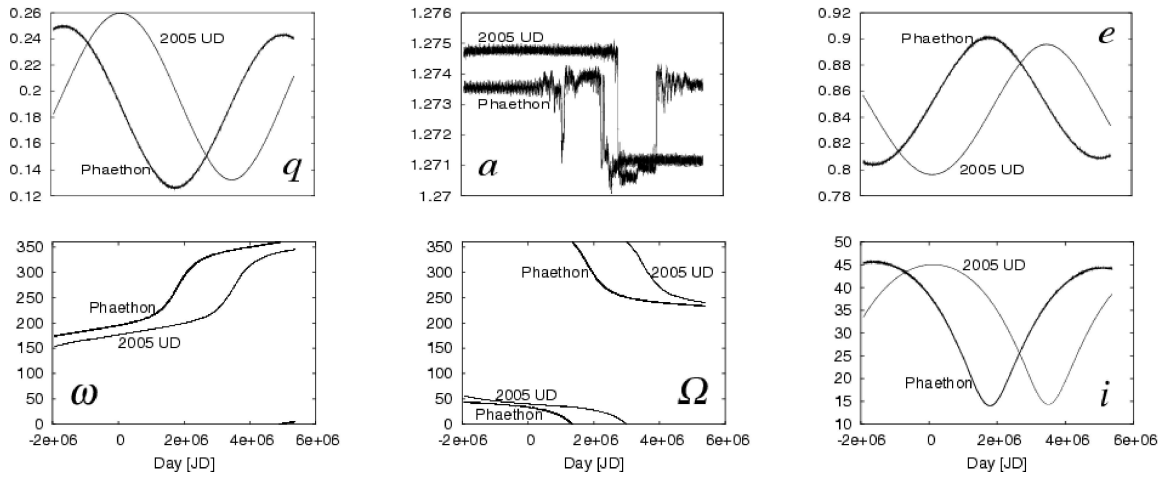

Figure 8.4 Dynamical evolution of (3200) Phaethon and 2005 UD for the six orbital elements, representing similar behavior with a time-shift of ∼4600 yr. The abscissa shows time in Julian Terrestrial Date (JTD). From Ohtsuka et al. (2006)

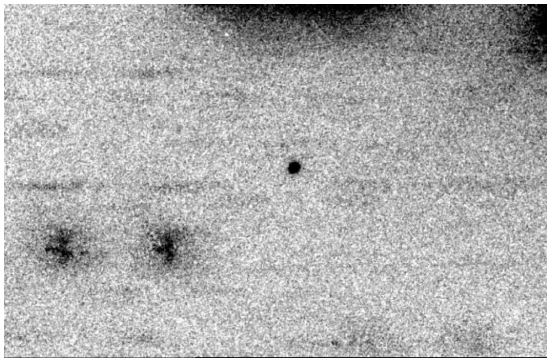

Figure 8.5 R-band image of 2005 UD in 1800 s exposure recorded using the UH2.2 on UT 2005 November 21. The region shown is ∼ 150" in width and the distances and phase angle of the object were $R = 1.59$ AU, $\Delta = 0.96$ AU and $\alpha = 35.8°$, respectively. From Jewitt and Hsieh (2006).

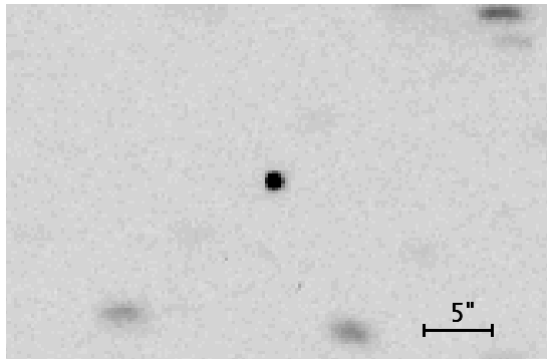

Figure 8.6 Keck telescope R-band image of 1999 YC on UT 2007 October 12 showing a point source with $FWHM \sim 0.65$" in 400 s integration, centered within a frame 40" wide. Heliocentric, geocentric distances and phase angle were $R = 2.60$ AU, $\Delta = 1.82$ AU and $\alpha = 16.4°$, respectively. From Kasuga and Jewitt (2008).

ability (de León et al., 2010, see also Todorović, 2018). However, the colors of Phaethon and Pallas are not strictly identical, as would be expected if one were an unprocessed chip from the other, although both are blue. Color differences might result from preferential heating and modification of Phaethon, with its much smaller perihelion distance (0.14 AU vs. ∼2.1 AU for Pallas). Recently, Ohtsuka et al. (2006, 2008a) suggested the existence of a "Phaethon-Geminid Complex (PGC)"–consisting of a group of dynamically associated split fragments, and identified the 1 km-sized asteroids 2005 UD and 1999 YC as having a common origin with Phaethon (cf. Figure 8.4). Photometry of 2005 UD and 1999 YC revealed the optical colors (Figures 8.5, 8.6). The former is another rare blue object (Jewitt and Hsieh, 2006; Kinoshita et al., 2007) while the latter is spectrally neutral (Kasuga and Jewitt, 2008) (see section 8.5.1).

The key question is how the Geminid meteoroid stream was produced from Phaethon. The extreme possibilities are that the Geminids are the products of a catastrophic event (for example an energetic collision, or a rotational disruption) or that they are produced in steady-state by continuing mass-loss from Phaethon.

In the steady-state case, the entire stream mass, $M_s \sim 10^{12}$ – 10^{13} kg (Hughes and McBride, 1989; Jenniskens, 1994; Blaauw, 2017)(cf. 1–2 orders larger in Ryabova, 2017), must be released over the last $\tau \sim 10^3$ years (the dynamical lifetime of the stream, cf. (Jones, 1978; Jones and Hawkes, 1986; Gustafson, 1989; Williams and Wu, 1993; Ryabova, 1999; Beech, 2002; Jakubík and Neslušan, 2015; Vaubaillon et al., 2019, Section 7.5.4)). This gives $dM_s/dt \sim M_s/\tau = 30$ – 300 kg s^{-1}, comparable to the mass loss rates exhibited by active Jupiter family comets. However, while the Jupiter family comets are notable for their distinctive comae of ejected dust, Phaethon generally appears as a point source, devoid of coma or other evidence for on-going mass loss (Chamberlin et al., 1996; Hsieh and Jewitt, 2005; Wiegert et al., 2008) (cf. Figure 8.3).

Recently, this general picture has changed with the detection of mass loss using near-perihelion observations taken

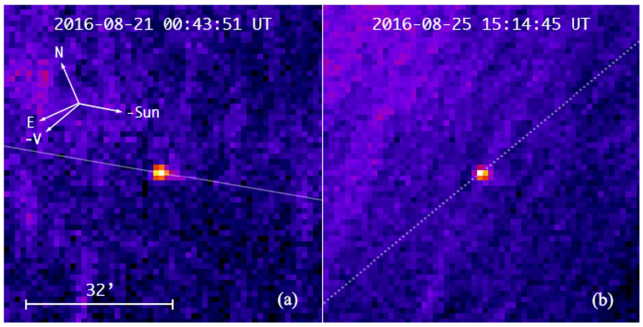

Figure 8.7 STEREO-A image taken on 2016 August 20 of (a) (3200) Phaethon and tail aligned on the position angles of the anti-solar direction and (b) the whole image sequence on the negative heliocentric velocity vector projected on the sky plane. Geometric parameters are $R \sim 0.14$ AU, Phaethon-STEREO distance ~ 0.9 AU, and the angle $\sim 120°$. The projected Sun-Phaethon line (the narrow white line across the left panel) is drawn to better illustrate that the direction of the tail was anti-solar, while the white dotted line across the right panel is the orientation. From Hui and Li (2017).

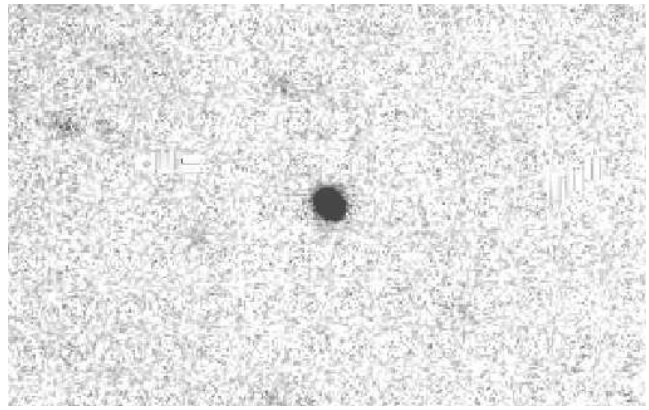

Figure 8.8 2003 EH_1 in a 360 s R-band image taken at Keck on UT 2013 October 2. No coma or tail is visible on the object having an FWHM of 0".86 in the frame of 40" × 25". R=2.1 AU, Δ=2.0 AU and α=27.6°. From Kasuga and Jewitt (2015).

with the Solar Terrestrial Relations Observatory (STEREO) spacecraft in 2009, 2012 and 2016 (Jewitt and Li, 2010; Jewitt et al., 2013; Li and Jewitt, 2013; Hui and Li, 2017). In addition to factor-of-two brightening at perihelion relative to the expected phase-darkened inverse-square law brightness, a diffuse, linear tail has been resolved, as shown in Figure 8.7. Because of its close association with the high temperatures experienced at perihelion, the activity is likely to result from thermal fracture or the desiccation of hydrated minerals. The observed particles from Phaethon are micron-sized, and are highly susceptible to solar radiation pressure sweeping. They are rapidly accelerated by radiation pressure and so cannot be retained in the Geminid stream (Jewitt and Li, 2010). In addition, their combined mass, $\sim 3 \times 10^5$ kg per perihelion, is at least $10^7\times$ smaller than the stream mass, M_s (Jewitt et al., 2013). It is possible that much more mass is contained in larger particles which, however, present a small fraction of the scattering cross-section and which, therefore, are unsampled in the optical data from STEREO.

In this regard, larger particles (sizes >10 μm) were recently reported in thermal emission at 25 μm (Arendt, 2014), but evidently contribute little to the optical scattering cross-section. The particles in the stream are estimated to be near mm-scale or larger (e.g. Blaauw, 2017), up to ∼1 to 10 cm, as measured in lunar impacts (Yanagisawa et al., 2008; Suggs et al., 2014; Ortiz et al., 2015; Szalay et al., 2018). The limit to optical depth of a Phaethon's trail is $\leq 3\times10^{-9}$ (Jewitt et al., 2018), consistent with those of cometary dust trails (10^{-9}–10^{-8}, from Sykes and Walker, 1992; Ishiguro et al., 2009) (see also section 8.6.3). While continued long wavelength observations of Phaethon to detect large particles will be helpful (Jewitt et al., 2015), the true nature of Phaethon and the PGC complex objects may await spacecraft missions resembling NASA's "Deep Impact" (A'Hearn et al., 2005; Kasuga et al., 2006, 2007a) and JAXA's "DESTINY+" (Sarli et al., 2018).

8.3.2 Quadrantids – 2003 EH_1

The Quadrantid meteor shower was first reported in 1835 (Quetelet, 1839) and appears annually in early January. The shower consists of two different components, the so-called young and old meteoroid streams, which represent a very short duration of core activity (lasting ∼0.5 day) and a broader, longer-lived (∼4 days) background activity (Wiegert and Brown, 2005; Brown et al., 2010, and references therein). The width of a meteoroid stream depends on its age, as a result of broadening by accumulated planetary perturbations. The small width of the Quadrantid core stream indicates ejection ages of only ∼200–500 years (Jenniskens, 2004; Williams et al., 2004; Abedin et al., 2015), and there is even some suggestion that the first reports of meteoroid stream activity coincide with the formation of the stream. On the other hand, the broader background stream implies larger ages of perhaps ∼3,500 years or more (Ohtsuka et al., 1995, 2008b; Kańuchová and Neslušan, 2007).

Two parent bodies of the Quadrantid complex have been proposed. The 4 km diameter Near-Earth Object (196256) 2003 EH_1 (hereafter 2003 EH_1), discovered on UT 2003 March 6 by the Lowell Observatory Near-Earth-Object Search (LONEOS) (Skiff, 2003), may be responsible for the young core stream (Jenniskens, 2004; Williams et al., 2004; Wiegert and Brown, 2005; Babadzhanov et al., 2008; Jopek, 2011; Abedin et al., 2015). The orbit of 2003 EH_1 has a = 3.123 AU, e = 0.619, i = 70°.838 and q = 1.191 AU (Table 8.1). The T_J (= 2.07) identifies it as a likely Jupiter family comet, albeit one in which on-going activity has yet to be detected (Koten et al., 2006; Babadzhanov et al., 2008; Borovička et al., 2009; Tancredi, 2014). The steady-state production rates $\lesssim 10^{-2}$ kg s^{-1} estimated from 2003 EH_1 at $R = 2.1$ AU are at least five orders of magnitude too small to supply the core Quadrantid stream mass $M_s \sim 10^{13}$ kg (Kasuga and Jewitt, 2015) (see Figure 8.8). Even at q=0.7–0.9 AU a few hundred years ago, sublimation-driven activity from the entire body takes ∼ 10s of years in the whole orbit, being hard to reconcile. In order to form the core Quadrantid

stream, we consider episodic replenishment by an unknown process to be more likely.

Comet 96P/Machholz 1 has been suggested as the source of the older, broader part of the Quadrantid complex (Vaubaillon et al., 2019, Section 7.5.2), with meteoroids released 2,000–5,000 years ago (McIntosh, 1990; Babadzhanov and Obrubov, 1991; Gonczi et al., 1992; Jones and Jones, 1993; Wiegert and Brown, 2005; Abedin et al., 2017, 2018). Comet 96P currently has a small perihelion orbit (a = 3.018 AU, e = 0.959, i = 59°.975 and q = 0.125 AU from Table 8.1) substantially different from that of 2003 EH_1. Despite this, calculations show rapid dynamical evolution that allows the possibility that 2003 EH_1 is a fragment of 96P, or that both were released from a precursor body (together defining the Machholz complex: Sekanina and Chodas, 2005). One or both of these bodies can be the parents of the Quadrantid meteoroids (Kańuchová and Neslušan, 2007; Babadzhanov et al., 2008; Neslušan et al., 2013a,b, 2014; Vaubaillon et al., 2019, Section 7.5.2).

A notable dynamical feature of 2003 EH_1 is the strong evolution of the perihelion distance (Wiegert and Brown, 2005; Neslušan et al., 2013b; Fernández et al., 2014). Numerical integrations indicate that the minimum perihelion distance $q \sim 0.12$ AU ($e \sim 0.96$) occurred ∼1500 yr ago (Neslušan et al., 2013b; Fernández et al., 2014), and the perihelion has increased approximately linearly with time from 0.2 AU 1000 years ago to the present-day value of 1.2 AU. At its recently very small (Phaethon-like) perihelion distance, it is reasonable to expect that the surface layers should have been heated to the point of fracture and desiccation (see section 8.5.4).

As described above, the Phaethon-produced Geminid meteoroids (q ∼0.14 AU) show extreme diversity in their Na abundance, from strong depletion to near sun-like Na content (Kasuga et al., 2005a; Borovička et al., 2005). Curiously, the Quadrantid meteoroids from the core stream are less depleted in Na than the majority of Geminid meteoroids (Koten et al., 2006; Borovička et al., 2009). The interpretation of this observation is unclear (see section 8.6.2).

The optical colors of 2003 EH_1 are similar to, but slightly redder than, those of the Sun. They are most taxonomically compatible with the colors of C-type asteroids (Kasuga and Jewitt, 2015) (see section 8.5.1).

8.3.3 Capricornids – 169P/NEAT

The α-Capricornids (CAP/1) are active from late July to early August, usually showing slow (∼22 km s^{-1}) and bright meteors. The shower, with an ascending nodal intersection of ω=270° with the Earth, is expected to be a twin stream also producing a daytime shower (Jenniskens, 2006). Because of the low entry velocities, the meteor plasma excitation temperature is $T_{ex} \lesssim$ 3600K and no trace of high temperature gas (i.e. hot component of $T_{ex} \sim 10^4$ K) is found (Borovicka and Weber, 1996). The metal contents of the α-Capricornids are unremarkable, being within a factor of a few of the Solar abundance (Borovicka and Weber, 1996; Madiedo et al., 2014).

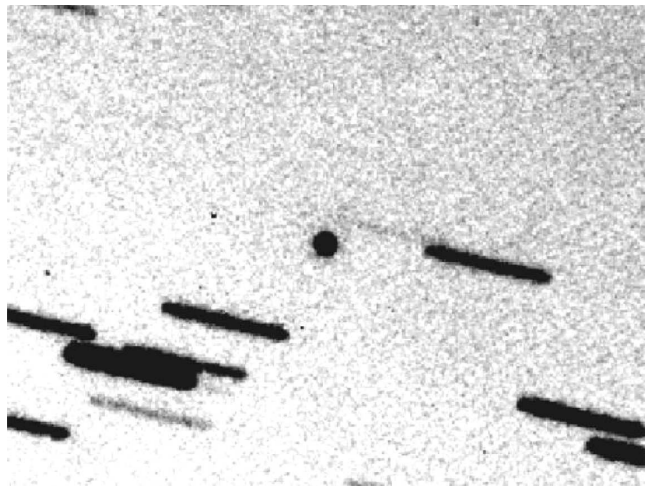

Figure 8.9 Comet 169P/NEAT in a 600 sec, r'-band image taken at the Dominion Astrophysical Observatory 1.8 m telescope on UT 2010 February 17. The frame size is $200'' \times 150''$. No coma or tail is visible on the object having an FWHM of 2.8". R=1.43 AU, Δ=0.47 AU and α=16.1°. From Kasuga et al. (2010).

Recently Brown et al. (2010) suggested that the Daytime Capricornids-Sagittariids (DCS/115) are closely dynamically related to the α-Capricornids. One of the parent body candidates, comet 169P/NEAT, has been identified as the parent body of the α-Capricornid meteoroid stream by numerical simulations (Jenniskens and Vaubaillon, 2010). The object was discovered as asteroid 2002 EX_{12} by the NEAT survey in 2002 (cf. Warner and Fitzsimmons, 2005; Green, 2005) and was re-designated as 169P/NEAT in 2005 after revealing a cometary appearance (Green, 2005). The orbital properties (Levison, 1996, T_J = 2.89) and optical observations reveal that 169P/NEAT is a ∼ 4 km diameter, nearly dormant Jupiter family comet with tiny mass-loss rate ∼ 10^{-2} kg s^{-1} (Kasuga et al., 2010) (Figure 8.9).

In the steady state, the stream mass M_s ∼10^{13}–10^{15} kg and the age τ∼5,000 yr (Jenniskens and Vaubaillon, 2010) together require a mass-loss rate four orders of magnitude larger than measured in 2010. In the case of 169P, cometary activity (a dust tail) was confirmed in 2005 (almost 1 orbital period before) and episodic mass-loss should be expected. This is a different case from other asteroidal parents of complexes. Kasuga et al. (2010) used the fractional change in the spin angular velocity to estimate the mass loss from 169P as ∼ 10^9–10^{10} kg per orbit. With the M_s and τ, the conclusion is that the origin of the α-Capricornids meteoroid stream could be formed by the steady disintegration of 169P.

Other parent body candidates continue to be proposed for the Capricornids. P/2003 T12 (SOHO) was suggested to share a common parent with 169P, following a breakup ∼2900 yr ago (Sosa and Fernández, 2015). Comet 169P is a large, almost inactive body (Kasuga et al., 2010), while P/2003 T12 seems to be a very small comet, with a sub-km radius nucleus (Sosa and Fernández, 2015) accompanied by dust-tails in near-Sun STEREO-B observations (Hui, 2013). The orbit of 2017 MB_1 was suggested to resemble that of

the α-Capricornids meteor shower (Wiegert et al., 2017). 2017 MB_1 has not been reported to show any sign of mass-loss activity.

8.3.4 Taurid Complex – 2P/Encke

The Taurid meteor shower includes the Northern, the Southern and other small branches (Vaubaillon et al., 2019, Section 7.5.5), possibly originating from more than one parent body. The Taurids show protracted, low-level activity with many fireballs from September to December, peaking in early November every year. The Taurid meteoroid complex has been suggested to be formed by a disrupted giant comet (40 km-sized) 10^4 years ago (Clube and Napier, 1984, 1987; Asher et al., 1993), although the very recent break-up of such a large (i.e. rare) body is statistically unlikely. Comet 2P/Encke has, for a long time, been considered as the most probable parent of the shower (Whipple, 1940).

The Taurid complex has a dispersed structure with low inclination and perihelia between 0.2 and 0.5 AU. The low inclination of the stream orbit enhances the effect of planetary perturbations from the terrestrial planets (Levison et al., 2006), resulting in the observed, diffuse structure of the complex (Matlovič et al., 2017). Furthermore, 2P has a relatively small heliocentric distance (aphelion is Q = 4.1AU) allowing it to stay mildly active around its orbit, and producing a larger spread in q ∼0.34 AU, than could be explained from ejection at perihelion alone (Gehrz et al., 2006; Kokotanekova et al., 2017).

An unfortunate artifact of the low inclination of the Taurid complex ($i \sim 12^\circ$, Table 8.1) is that many near-Earth asteroids are plausible parent bodies based on orbital dynamical calculations (e.g. Asher et al., 1993; Steel and Asher, 1996; Babadzhanov, 2001; Porubčan et al., 2004, 2006; Babadzhanov et al., 2008). As a result, many of the proposed associations are likely coincidental (Spurný et al., 2017; Matlovič et al., 2017). Actually no spectroscopic linkage between 2P/Encke and the 10 potential Taurid-complex NEOs has been confirmed (the latter are classified variously as X, S, Q, C, V, O, and K-types) (Popescu et al., 2014; Tubiana et al., 2015), this being totally different from the case of the Phaethon-Geminid Complex. Here, we focus on the physical properties of the Taurid meteor shower and the most strongly associated parent, 2P/Encke.

Spectroscopic studies of some Taurid meteors find a carbonaceous feature (Borovička, 2007; Matlovič et al., 2017). The heterogeneity (large dispersion of Fe content) and low strength (0.02–0.10 MPa) of the Taurids (Borovička et al., 2019, Section 2.3.4) suggest a cometary origin, consistent with but not proving 2P as a parent (Borovička, 2007; Matlovič et al., 2017). Note that the current perihelion distance (q ∼0.34 AU, where $T \sim 480$ K) is too large for strong thermal metamorphism to be expected (Borovička, 2007).

Comet 2P/Encke is one of the best characterized short-period comets, with published determinations of its rotation period, color, albedo and phase function (see reviews; Lamy et al., 2004; Kokotanekova et al., 2017). For example, the effective radius is 2.4 km, the average color indices, $B - V = 0.73 \pm 0.06$ and $V - R = 0.39 \pm 0.06$ (e.g. Lowry and Weissman, 2007b), the rotational period is about 11 hr or 22 hr (but changing with time in response to outgassing torques (Belton et al., 2005; Kokotanekova et al., 2017, and references therein); with minimum axis ratio 1.4 (Fernández et al., 2000; Lowry and Weissman, 2007a; see also, Lamy et al., 2004).

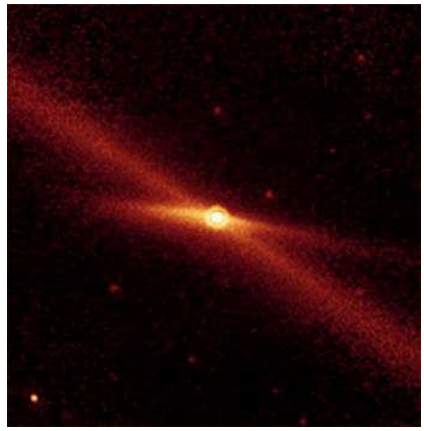

Figure 8.10 The 24 μm infrared image of comet 2P/Encke obtained in 2004 June by the Spitzer Space Telescope. The image field of view is about 6' and centered on the nucleus. The near horizontal emission is produced by recent cometary activity, and the diagonal emission across the image is the meteoroid stream along the orbit (Kelley et al.,2006; see also Reach et al., 2007). Courtesy NASA/JPL-Caltech/M. Kelley (Univ. of Minnesota).

Optically, 2P appears dust-poor because optically bright micron and sub-micron sized dust particles are underabundant in its coma (Jewitt, 2004a). However, the dust / gas ratio determined from thermal emission is an extraordinary $\mu \sim 30$, suggesting a dust-rich body (Reach et al., 2000; Lisse et al., 2004) compared to, for example, Jupiter family comet 67P/Churyumov-Gerasimenko, where $\mu = 4 \pm 2$ (Rotundi et al., 2015). The total mass loss is 2–6 $\times$ 10^{10} kg per orbit, mostly in the form of large particles that spread around the orbit and give rise to 2P's thermal dust trail as the source of Taurid meteor showers (Asher and Clube, 1997; Reach et al., 2000) (see Figure 8.10). The entire structured stream mass, $M_s \sim 10^{14}$ kg (Asher et al., 1994), must have been released over the last $\tau \sim$ 5,000 – 20,000 years (the dynamical lifetime of the stream, cf. Whipple, 1940; Babadzhanov and Obrubov, 1992a; Jenniskens, 2006). This gives $dM_s/dt \sim M_s/\tau = 200$ – 600 kg s^{-1}, a few times larger than the mass loss rates typically reported for active Jupiter family comets. Various small near-Earth objects and some meteorite falls have been linked with the orbit of the stream as potentially hazardous (Brown et al., 2013; Olech et al., 2017; Spurný et al., 2017).

8.3.5 Sekanina's (1973) Taurids-Perseids – Icarus

The Icarus asteroid family was reported as the first family found in the near-Earth region, which dynamically relates asteroids 1566 Icarus, 2007 MK_6 and Sekanina's (1973) Taurid-Perseid meteor shower (Ohtsuka et al., 2007) (see Figure 8.11).

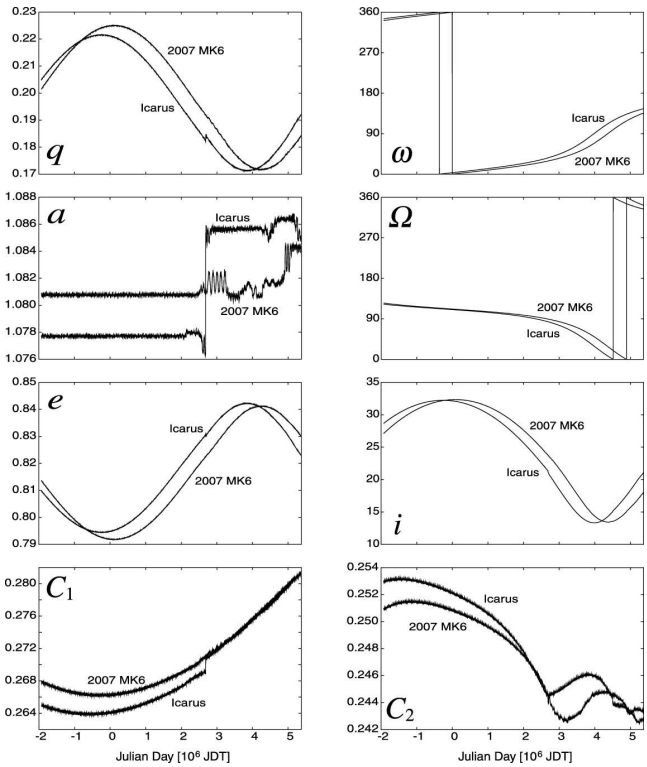

Figure 8.11 Dynamical evolution process of 1566 Icarus and 2007 MK_6 in JTD. The orbital elements (q, a, e, ω, Ω and i) and the C_1 and C_2 integrals are plotted (cf. Table 8.1). Time-shifting is only ∼1,000 yr. From Ohtsuka et al. (2007).

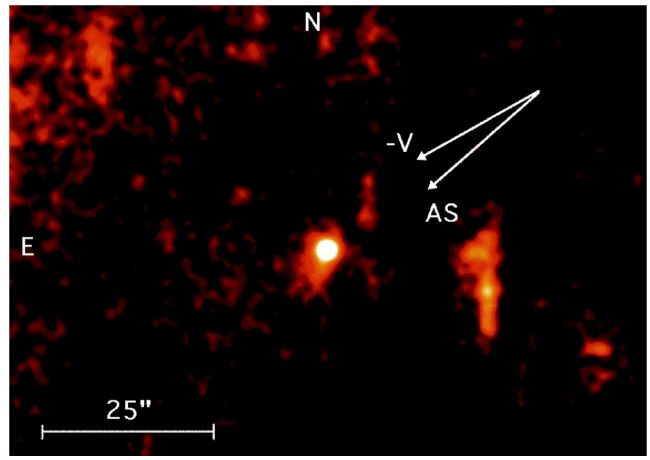

Figure 8.12 2003 WY_{25} (=289P/Blanpain) imaged in R-band, 500 sec integration at R=1.6 AU, Δ=0.7 AU and α=20.7° using UH2.2 on UT 2004 March 20. A faint coma is apparent, extending to the southeast. Arrows show the directions of the negative heliocentric velocity vector (marked "-V") and the anti-solar direction ("AS"). The estimated radius ∼ 160 m is the smallest active cometary parent ever observed. From Jewitt (2006).

Near-Earth Apollo asteroid 1566 Icarus (= 1949 MA) was discovered in 1949, having distinctive small q=0.19 AU and high i=23° (Baade et al., 1950). The object has diameter D_e∼ 1 km (e.g. Table 1, from Chapman et al., 1994), a moderately high albedo of 0.30 – 0.50 (cf. Gehrels et al., 1970; Veeder et al., 1989; Chapman et al., 1994; Nugent et al., 2015) and a short rotational period, ∼2.273 hr (e.g. Miner and Young, 1969) (see also, Harris and Lagerros, 2002). A reflection spectrum close to Q- or V-type asteroids is found (Gehrels et al., 1970; Hicks et al., 1998; Dundon, 2005) (see section 8.5.1).

On the other hand, near-Earth asteroid 2007 MK_6 (= 2006 KT_{67}) was discovered in 2007 (Hill et al., 2007). Assuming an albedo like that of Icarus, then 2007 MK_6 is ∼180 m in diameter as computed from the absolute magnitude H=20.3 (MPO386777) (see Table 8.2). The breakup hypothesis from Icarus, if true, could be due to near a critical rotation period and thermal stress induced at small q∼0.19 AU (subsolar temperature ∼ 900 K), which might be related to the production of the meteoroid stream (see section 8.5.2). The Taurid-Perseid meteoroids can be dynamically related with the Icarus asteroid family (D_{SH} ∼ 0.08), speculated to cross the Earth's orbit (Sekanina, 1973). The rare detection of the Taurid-Perseid meteor shower may result from the intermittent stream (swarm) due to very limited dust supply phase from the parent body.

8.4 Possible Complexes

Here, we describe two examples of less well-characterized complexes suspected to include stream branches and one or more parent bodies.

8.4.1 Phoenicids – Comet D/1819 W1 (Blanpain)

The Phoenicid meteor shower was first reported more than 50 years ago, on December 5 in 1956 (Huruhata and Nakamura, 1957). Promptly, the lost Jupiter family comet D/1819 W1 (289P/Blanpain) was proposed as the potential source (Ridley, 1957 reviewed in Ridley, 1963). In 2003, the planet-crossing asteroid 2003 WY_{25} was discovered (Ticha et al., 2003), with orbital elements resembling those of D/Blanpain (Foglia et al., 2005; Micheli, 2005). The related Phoenicids' activity in 1956 and 2014 (Watanabe et al., 2005; Jenniskens and Lyytinen, 2005; Sato et al., 2017; Tsuchiya et al., 2017), raised the possibility that 2003 WY_{25} might be either the dead nucleus of D/Blanpain itself or a remnant of the nucleus surviving from an earlier, unseen disintegration. Jewitt (2006) optically observed asteroid 2003 WY_{25}, finding the radius of 160 m (an order of magnitude smaller than typical cometary nuclei), and revealing a weak coma consistent with mass-loss rates of 10^{-2} kg s^{-1} (Figure 8.12). The latter is too small to supply the estimated 10^{11} kg stream mass on reasonable timescales (≤10,000 yrs, Jenniskens and Lyytinen, 2005). Indeed, the mass of 2003 WY_{25} (assuming density 1000 kg m^{-3} and a spherical shape) is ∼2×10^{10} kg, smaller than the stream mass. Either the stream was produced impulsively by the final stages of the break-up of a once much larger precursor to 2003 WY_{25}, or another parent body may await discovery (Jewitt, 2006).

8.4.2 Andromedids – Comet 3D/Biela

The Andromedid meteor shower (AND/18) was firstly reported in 1798 (Hawkins et al., 1959). The dynamics were linked with Jupiter family comet 3D/Biela (Kronk, 1988, 1999). The shower is proposed to result from continuous disintegration of 3D/Biela from 1842 until its sudden disappearance in 1852, resulting in irregular meteor shower appearances (e.g. Olivier, 1925; Cook, 1973; Jenniskens and Vaubaillon, 2007). The estimated stream mass is 10^{10} kg (Jenniskens and Lyytinen, 2005), however, the absence of parent candidates means that little can be determined about the production of the meteoroids. Nonetheless, the Andromedid meteor shower was actually detected by radar in 2011 and is numerically predicted to appear in the coming decades (Wiegert et al., 2013).

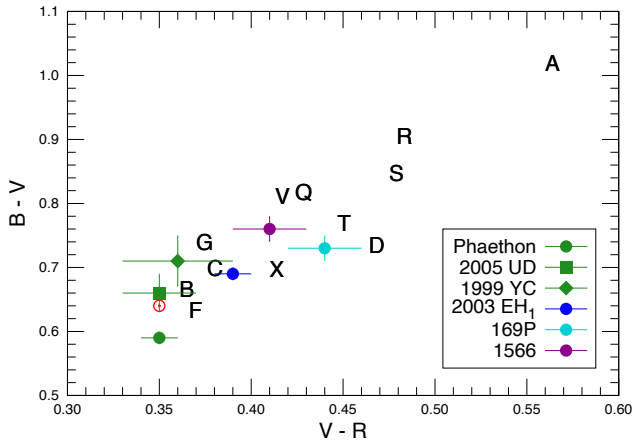

Figure 8.13 Color plots of $V-R$ vs. $B-V$ showing parent bodies (filled symbols) from Table 8.2, and Tholen taxonomic classifications (Tholen, 1984), as tabulated by Dandy et al. (2003). The color of the Sun (red circle) is also plotted.

8.5 Parent Bodies

In this section we discuss group physical properties of the parent bodies (cf. Table 8.2). Most objects (e.g. 3200 Phaethon, 2005 UD, 1999 YC, 2003 EH_1 and 169P) show point-like images (Figures 8.3, 8.5, 8.6, 8.8, 8.9) from which we can be confident that the measured properties refer to the bare objects (or nuclei) alone. However, 2P/Encke, 2003 WY_{25} and some other comets may sometimes be active (e.g. Figures 8.10, 8.12) leading to potential confusion between the properties of the nucleus and the near-nucleus comae.

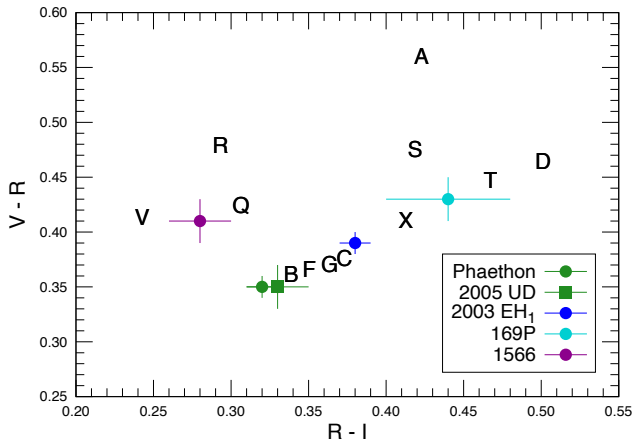

Figure 8.14 The same as Figure 8.13 but in the $R-I$ vs. $V-R$ color plane. The color of the Sun is exactly coincident with that of 2005 UD.

8.5.1 Colors

Figures 8.13 and 8.14 show distributions of the colors of the parent bodies from Table 8.2. In addition, Tholen taxonomy classes are plotted from photometry of NEOs from Dandy et al. (2003). Here, 2P is not included because of the coma contamination suggesting mild activity during the whole orbit.

The asteroids of the PGC (3200 and 2005 UD, 1999 YC) show colors from nearly neutral to blue. Asteroids 3200 Phaethon and 2005 UD are classified as B-type asteroids (cf. Dundon, 2005; Jewitt and Hsieh, 2006; Kinoshita et al., 2007; Licandro et al., 2007; Kasuga and Jewitt, 2008; Jewitt, 2013; Ansdell et al., 2014), while 1999 YC is a C-type asteroid (Kasuga and Jewitt, 2008). Heterogeneity on the surfaces of Phaethon and 2005 UD may be due to intrinsically inhomogeneous composition, perhaps affected by hydration processes (Licandro et al., 2007), and by thermal alteration (Kinoshita et al., 2007). The rotational color variation of 2005 UD shows B-type for 75% of the rotational phase but C-type for the remainder (Kinoshita et al., 2007). The colors of the PGC objects are broadly consistent with being neutral-blue.

Optical colors of 2003 EH_1 are taxonomically compatible with those of C-type asteroids (Kasuga and Jewitt, 2015) (Figures 8.13 and 8.14). The V-R color (0.39±0.01) is similar to that of 96P ($V-R=0.40\pm0.03$, from Licandro et al., 2000; Meech et al., 2004). We note that the optical colors of 2003 EH_1 are significantly less red than the average colors of cometary nuclei (Jewitt, 2002; Lamy et al., 2004). This could be a result of past thermal processing when the object had a perihelion far inside Earth's orbit. Indeed, the weighted mean color of 8 near-Sun asteroids having perihelion distances $\lesssim 0.25$ AU (subsolar temperatures $\gtrsim 800$ K) is V-R = 0.36±0.01 (Jewitt, 2013), consistent with the color of EH_1 (cf. section 8.5.4).

The optical colors measured for 169P/NEAT are less red than D-type objects, as found in normal cometary nuclei and Trojans, but similar to those of T- and X- type asteroids (Figures 8.13 and 8.14). The near-infrared spectrum measurement (0.8–2.5 μm) classified 169P as a T-type asteroid based on the Bus taxonomy with p_v=0.03±0.01 (DeMeo and Binzel, 2008). The T-type asteroids represent slightly redder-sloped visible wavelength spectra than those of C-type. Perhaps a refractory rubble mantle has formed on the

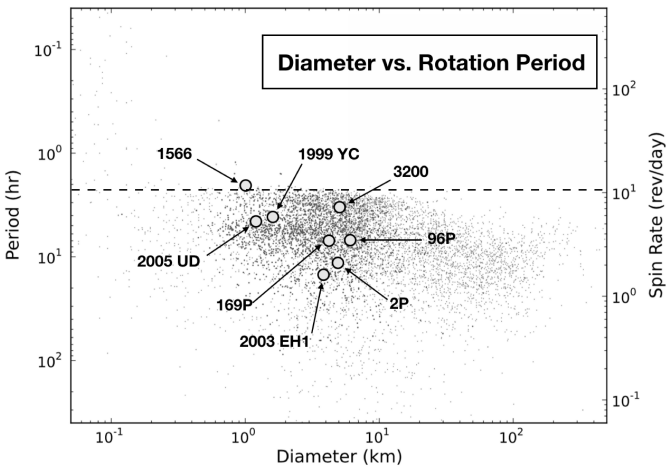

Figure 8.15 Diameter vs. rotational period for asteroids (dots) and the parent bodies of meteoroid streams (large circles). The asteroid data are taken from Chang et al. (2015) while the parent body parameters are listed in Table 8.2. The horizontal dotted line shows the spin barrier period of ∼2.2 hr (e.g. Warner et al., 2009) and asteroid 1566 Icarus rotates nearby.

169P surface, driven by volatile sublimation, and red matter has been lost (Jewitt, 2002).

Asteroid 1566 Icarus is taxonomically classified as a Q- or V-type (Figures 8.13 and 8.14). These types suggest thermal evolution (perhaps at the level of the ordinary chondrites) relative to the more primitive carbonaceous chondrites. The formation process of the associated complex is unknown, but we speculate that processes other than comet-like sublimation of ice are responsible.

8.5.2 Dust Production Mechanism: Example of 1566 Icarus and 2007 MK_6

Here we consider possible dust production mechanisms from asteroidal parents. A diameter – rotation plot compiled from the data in Table 8.2 is shown in Figure 8.15. The rotational period of 1566 Icarus ($P_{\rm rot}$=2.273 hr) is near the spin barrier period of ∼2.2 hr (Warner et al., 2009; Chang et al., 2015). Asteroids rotating near or faster than this barrier are presumed to have been destroyed when centrifugal forces have overcome the gravitational and cohesive forces binding them together (Pravec et al., 2008).

The aftermaths of recent and on-going asteroid break-up have been identified observationally (e.g. P/2013 R3, Jewitt et al., 2014, 2017) and studied theoretically (Hirabayashi et al., 2014). Additionally, different mechanisms can operate together. Rotational instability in P/2013 R3, for instance, might have been induced by YORP torques, or by outgassing torques from sublimated ice, or by a combination of the two. Thermal disintegration, electrostatic ejection and radiation pressure sweeping may all occur together on near-Sun object 3200 Phaethon (Jewitt and Li, 2010). Figure 8.15 shows that 1566 rotates near the ∼2.2 hr spin barrier period, implying a rotational breakup in the past. Both 1566 and its possible fragment 2007 MK_6 have small perihelia (q ∼0.19 AU). We consider rotational instability as a possible cause of their past separation.

In principle, rotation rates of asteroids can be accelerated to critical limits by torques exerted from solar radiation through the YORP effect (Vokrouhlický et al., 2015). The YORP e-folding timescale of the spin, $\tau_{\rm Y}$, is estimated from the ratio of the rotational angular momentum, L, to the torque, T. The relation may be simply expressed as $\tau_{\rm Y} \sim K\, D_e^2\, R_h^2$ (Jewitt et al., 2015), where K is a constant, D_e is the asteroid diameter (km) and R_h is the heliocentric distance (AU). The value of constant K is sensitive to many unknown parameters (the body shape, surface texture, thermal properties and spin vector of the asteroid and so on), but can be experimentally estimated from published measurements of YORP acceleration in seven well-characterized asteroids (Table 2 from Rozitis and Green, 2013). Scaling K to the bulk density of 1566 Icarus $\rho = 3400\,{\rm kg\,m^{-3}}$ (V-type or ordinary chondrite from Wilkison and Robinson, 2000; Britt et al., 2002) and its rotation period $P_{\rm rot}$=2.273 hr, we find $K \sim 7{\times}10^{13}\,{\rm s\,km^{-2}\,AU^{-2}}$. The approximation is represented as (cf. Equation (3) of Jewitt et al., 2015),

$$\tau_Y\ ({\rm Myr}) \approx 2 \left[\frac{\rm D_e}{1\,{\rm km}}\right]^2 \left[\frac{\rm R_h}{1\,{\rm AU}}\right]^2 . \qquad (8.4)$$

For 1566 with D_e=1 km orbiting at R_h ∼1.08 AU, Equation (8.4) gives $\tau_{\rm Y} \approx 2$ Myr. This is two orders of magnitude smaller than the collisional lifetime of 1-km near-Earth asteroids (Bottke et al., 1994), suggesting that YORP torque spin-up is plausible.

Asteroids rotating faster than the spin-barrier cannot be held together by self-gravitation only, but require cohesive strength (e.g. Scheeres et al., 2010). The cohesive strength at rotational breakup of a body can be estimated by the dispersed fragmental sizes, initial separation speed, and the bulk density using Equation (5) of Jewitt et al. (2015),

$$S \sim \rho \left(\frac{D_e^{'}}{D_e}\right) (\Delta v)^2. \qquad (8.5)$$

Both fragmental asteroids (1566 and 2007 MK_6) are assumed to have the same bulk density ρ, D_e and $D_e^{'}$ are diameters of 1566 and 2007 MK_6 respectively (see Table 8.2), and Δv is the excess velocity of escaping fragments, assumed comparable to the escape velocity from 1566. Adopting the same value for ρ (see above) and substituting $(D_e^{'}/D_e)$ = 0.18 (the diameter ratio between MK_6 and 1566), and Δv = $0.69\,{\rm m\,s^{-1}}$, we find $S \sim 290\,{\rm N\,m^{-2}}$.

This small value is comparable to strengths ∼10–$100\,{\rm N\,m^{-2}}$ modeled by a rubble-pile asteroid bounded by weak van der Waals forces (reviewed in Scheeres and Sánchez, 2018), but more than five orders of magnitude smaller than the values of typical competent rocks (10^7 – 10^8 ${\rm N\,m^{-2}}$). A rotational break-up origin of 1566 and MK_6 is possible provided they have a weak, rubble-pile structure, as is thought likely for a majority of kilometer-sized asteroids as a result of past, non-destructive impacts.

Several processes could eject dust from the surface of 1566. Firstly, thermal disintegration can be induced by thermal expansion forces that make cracks on the surfaces of aster-

oids and produce dust particles. The characteristic speeds of dust particles produced by disintegration can be derived by conversion from thermal strain energy into kinetic energy of ejected dust particles. The necessary conversion efficiency, η, is given by (cf. Equation (3) of Jewitt and Li, 2010)

$$\eta \sim \left(\frac{v_e}{\alpha\,\delta T}\right)^2 \left(\frac{\rho}{Y}\right), \tag{8.6}$$

where, $v_e = 0.69\,\mathrm{m\,s^{-1}}$ is the escape velocity from 1566, $\alpha \sim 10^{-5}\,\mathrm{K^{-1}}$ is the characteristic thermal expansivity of rock (Lauriello, 1974; Richter and Simmons, 1974), $\delta T \sim$450 K is the temperature variation between the q and Q, and $Y = (1\text{–}10) \times 10^{10}\ \mathrm{N\,m^{-2}}$ are typical Young's moduli for rock (Pariseau, 2006, p.474). With ρ as above we find $\eta \gtrsim 0.1$–1 % is needed for the velocities of ejected dust particles to surpass the escape velocity. This very small value of conversion efficiency is sufficient for most dust particles produced by thermal disintegration to be launched into interplanetary space.

Secondly, electrostatic forces caused by photoionization by solar UV can eject small particles. The critical size for a 1 km-diameter asteroid is $a_e \lesssim 4\ \mu$m (Equation (12) Jewitt et al., 2015). Millimeter-sized particles cannot be electrostatically launched and this process may contribute little or nothing to meteoroid stream formation.

Finally, radiation pressure sweeping can remove small particles from an asteroid once they are detached from the surface by another process (i.e. once the surface contact forces are temporarily broken). Radiation pressure sweeping is most effective at small heliocentric distances. The critical size to be swept away, $a_{\rm rad}$ (μm), is estimated by equating the net surface acceleration (gravitational and centripetal) with the acceleration due to radiation pressure, given by Equation (6) of Jewitt and Li (2010)

$$a_{\rm rad} \sim \frac{3\,g_\odot}{2\,\pi\,R_{\rm AU}^2\,f^{1/2}\,D_e}\left[\frac{G\,\rho}{f^2} - \frac{3\,\pi}{P_{\rm rot}^2}\right]^{-1}, \tag{8.7}$$

where, $g_\odot$ is the gravitational acceleration to the Sun at 1 AU, $R_{\rm AU}$ is the heliocentric distance expressed in AU, f is the limit to the axis ratio (=a/b), G is the gravitational constant. We substitute $g_\odot = 0.006\,\mathrm{m\,s^{-2}}$, $R_{\rm AU} = 0.187$ (Table 8.1), f=1.2 (Table 8.2), $G = 6.67 \times 10^{-11}\mathrm{m^3\,kg^{-1}\,s^{-2}}$ and adopt the same values of D_e, ρ and $P_{\rm rot}$ (see above) into Equation (8.7), then obtain $a_{\rm rad} \sim$ 4,500 μm $\approx$ 5 mm. This size is large enough to contribute meteoroid-sized particles to a stream (see 8.6.3, Meteoroid Streams).

In summary, asteroid 1566 Icarus is a possible product of rotational breakup and, given its small perihelion distance, potentially experiences a mass loss process similar to those inferred on Phaethon. Near-perihelion observations of 1566 and/or 2007 $\mathrm{MK_6}$ may indeed show Phaethon-like mass-loss.

8.5.3 End State

Active objects on comet-like orbits with $T_J < 3.08$ (Table 8.1 and Figure 8.1) are presumed to be potential ice sublimators. The timescales for the loss of ice from a mantled body $\tau_{\rm dv}$, for the heat propagation into the interior of a body $\tau_{\rm c}$, and dynamical lifetime of short-period comets $\tau_{\rm sp} \sim 10^5$–10^6 yr (Duncan et al., 2004) can be compared to predict an object's end state (Jewitt, 2004b).

The $\tau_{\rm dv}$ is calculated using $\rho_{\rm n} D_e/2f(dm/dt)$, where $\rho_{\rm n} = 600\,\mathrm{kg\,m^{-3}}$ is the cometary bulk density (Weissman et al., 2004) and $f = 0.01$ is the mantle fraction (A'Hearn et al., 1995). The orbit with averaged $\bar{a} \sim 2.7$ AU and $\bar{e} \sim 0.8$ from the seven objects has a specific mass loss rate of water ice $dm/dt \lesssim 10^{-4}\,\mathrm{kg\,m^{-2}\,s^{-1}}$ (Figure 6, in Jewitt, 2004b). Then we find $\tau_{\rm dv} \gtrsim 10^4\ D_e$ in yr, where D_e is an effective diameter in km (Table 8.2). The $\tau_{\rm c} \sim 8.0{\times}10^4\ D_e^2$ in yr is derived from the equation of heat conduction given by $D_e^2/4\kappa$, where $\kappa = 10^{-7}\,\mathrm{m^2\,s^{-1}}$ is the assumed thermal diffusivity of a porous object. The critical size of object to form an inactive, devolatilized surface is constrained by the relation $\tau_{\rm dv} \lesssim \tau_{\rm c}$, which gives $D_e \gtrsim 0.13$ km. Likewise, the size capable of containing ice in the interior of a body for the dynamical lifetime is given by the relation $\tau_{\rm c} \gtrsim \tau_{\rm sp}$, which gives $D_e \gtrsim 1.1$ km.

Most comet-like objects are expected to be dormant, with ice depleted from the surface region, but potentially still packed deep inside. We note that 2003 $\mathrm{WY_{25}}$ of the Phoenicids is on its way to the dead state due to its small size ($D_e = 0.32$ km). The $\tau_{\rm c} \sim$ 8,000 yr suggests that solar heat can reach into the body core approximately 1 or 2 orders of magnitude sooner than the end of the dynamical lifetime. The core temperature around the orbit (Jewitt and Hsieh, 2006), $T_{\rm core} \sim 180$ K, exceeds the sublimation temperature of water ice 150 K (Yamamoto, 1985). The extremely weak activity of 2003 $\mathrm{WY_{25}}$ may portend its imminent demise (cf. section 8.4.1).

8.5.4 Lidov-Kozai Mechanism[2]

The Lidov-Kozai mechanism works on the secular dynamics of small solar system objects. Large-amplitude periodic oscillations of the e and i (in antiphase) are produced, whereas the a is approximately conserved, while the ω librates around $\pi/2$ or $3\pi/2$ if $C_2 < 0$ or circulates if $C_2 > 0$ (Kozai, 1962; Lidov, 1962).

Perihelia can be deflected into the vicinity of the Sun by this mechanism (on timescale ∼1000s of years), perhaps causing physical alteration (or even breakup) due to enormous solar heating (Emel'yanenko, 2017). We find all parent bodies stay in the circulation region ($C_2 > 0$, see Table 8.1). The minimum perihelion distance $q_{\rm min}$ can be computed using maximum eccentricity, $e_{\rm max}$, given by (Equations (5) and (28) of Antognini (2015))

$$e_{\rm max} = \sqrt{1 - \frac{1}{6}\left(\zeta - \sqrt{\zeta^2 - 60\,C_1}\right)}, \tag{8.8}$$

where $\zeta = 3{+}5(C_1{+}C_2)$ (Equation (31) of Antognini, 2015), C_1 and C_2 are from Table 8.1. With the obtained $q_{\rm min}$, we find the Geminids (PGC), Quadrantids and Sekanina's (1973) Taurid-Perseids complexes are near-Sun objects (Table 8.3). Amongst them, 2003 $\mathrm{EH_1}$ turns itself into a near-Sun object with $q_{\rm min} \sim$ 0.12 AU (cf. section 8.3.2), albeit

[2] In Chapter 7 (Vaubaillon et al., 2019) the Lidov-Kozai mechanism focuses on secular changes in e, i and ω to find how e and ω relate to whether an orbit intersects Earth's orbit to produce a meteor shower.

Table 8.3. *Closest Approach to the Sun by the Lidov-Kozai Mechanism*

Complex	Object	$e_{\max}$[a]	$q_{\min}$[b]	$T_{\rm peak}$[c]	Ref.[d]
Geminids	Phaethon	0.90	0.13	1100	∼0.13[1]
	2005 UD	0.90	0.13	1100	0.13–0.14[1]
	1999 YC	0.89	0.16	1000	-
Quadrantids	2003 EH_1	0.96	0.12	1100	∼0.12[2]
	96P/Machholz 1	0.99	0.03	2300	0.03–0.05[3]
Taurids-Perseids	1566 Icarus	0.85	0.16	1000	∼0.17[4]
	2007 MK_6	0.85	0.16	1000	∼0.17[4]

Notes: Near-Sun objects have perihelia $\lesssim 0.25$ AU.
[a] Maximum eccentricity (Equation (8.8))
[b] Minimum perihelion distance (AU) estimated by $\simeq a(1-e_{\max})$, where a is from Table 8.1.
[c] Peak temperature at $q_{\min}$ (K)
[d] Referred minimum perihelion distance (AU) from numerical integrations and analytical methods
[1]Ohtsuka et al. (1997, 2006) (cf. Figure 8.4) [2]Neslušan et al. (2013b); Fernández et al. (2014) (see section 8.3.2) [3]Bailey et al. (1992); Sekanina and Chodas (2005); Abedin et al. (2018) [4]Ohtsuka et al. (2007) (cf. Figure 8.11)

$q \sim 1.2$ AU at present (see Figure 8.1). The peak temperature $\gtrsim 1000$ K is similar to that experienced by Phaethon (cf. 1566 Icarus), and could likewise cause strong thermal and desiccation stresses, cracking and alteration in EH_1, with the release of dust (Jewitt and Li, 2010; Molaro et al., 2015; Springmann et al., 2018). This example reminds us that, even in objects with q presently far from the Sun, we cannot exclude the action of extreme thermal processes in past orbits.

8.6 Meteors and Streams

8.6.1 Na Loss: Thermal

Sodium loss in Geminid meteors results from the action of a thermal process in or on the parent body, Phaethon (section 8.3.1). Čapek and Borovička (2009) calculated the timescale for thermal depletion of Na from an assumed initial solar value down to 10% of solar abundance in Geminid meteoroids during their orbital motion in interplanetary space (using assumed albite ($NaAlSi_3O_8$) and orthoclase ($KAlSi_3O_8$) compositions). With particle diameters $\geq$ mm-scale, they found depletion timescales $\gtrsim 10^4$–10^5 yr (Figure 8.16), some 1 to 2 orders of magnitude longer than the stream age of $\lesssim 10^3$ yr. On the other hand, the dynamical lifetime of Phaethon, while very uncertain, is estimated to be $\sim 3 \times 10^7$ yr (de León et al., 2010). This is surely long compared to the age of the Geminid stream and long enough for Na to be thermally depleted from Phaethon.

In principle, other processes might affect the sodium abundance. Sputtering by the solar wind, photon stimulated Na desorption (on Mercury and the Moon) (McGrath et al., 1986; Potter et al., 2000; Killen et al., 2004; Yakshinskiy and Madey, 2004) and cosmic ray bombardment (Sasaki et al., 2001) have been well studied. These processes act only on the surface, and are inefficient in removing Na from deeper layers (Čapek and Borovička, 2009).

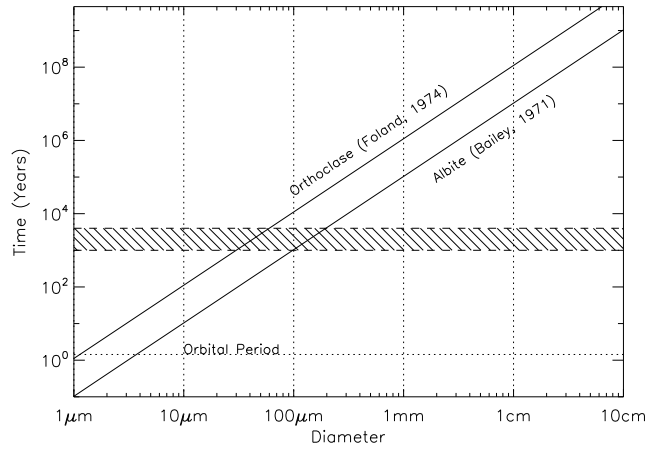

Figure 8.16 Timescale for escape of 90% of initial Na content from Geminid meteoroids in the stream, as a function of the meteoroid size. The low diffusion data for Na in orthoclase was used as a limit for the slowest loss, while the faster diffusion data for Na in albite (10× higher than for orthoclase) is considered as a more realistic value for the Geminids. The time interval in the shaded region corresponds to the estimated age of the Geminid meteoroid stream (1000–4000 yr). From Čapek and Borovička (2009).

8.6.2 Abundances vs. Intensity Ratios

In the interpretation of meteor spectra, two types of evaluation methods are employed in the literature. Some investigators calculate elemental abundances while others use simple line intensity ratios. Here we describe advantages and disadvantages hidden in both methods.

Elemental abundances are quantitatively utilized for comparing with those of meteor showers and the solar abundances (Anders and Grevesse, 1989; Lodders, 2003). The derivation of abundances is influenced by the complicated physics of the ionized gas at the head of the meteor (Borovicka, 1993; Kasuga et al., 2005b). For example, the Saha equation is needed to calculate the neutral vs. ion balance, but this depends on the assumption of a plausible excitation temperature, T_{ex}, for the emitting region. This is par-

ticularly important for Na, which has a smaller first ionization energy (≈ 5.1 eV) compared to other species (e.g. Mg: $\approx$ 7.6 eV, Fe: ≈ 7.9 eV). The selection of the appropriate T_{ex} is problematic. Fireball-like spectra have been suggested to be the combination of some thermal components with typical $T_{ex} \sim$ 5,000, 8,000 and 10,000 K, respectively (Borovicka, 1993; Kasuga et al., 2005b, 2007b). Borovicka (1993) considered Ca II lines in the hot components ($T_{ex} \sim$ 10,000 K) and estimated electron density from the radiating volume of the meteor in the direction of its flight. This implies that Ca II may not reflect the actual electron density from their spectral emission profile. In Kasuga et al. (2005b), on the other hand, Ca II is taken from the main component ($T_{ex} \sim$ 5,000 K) instead of the hot one, and they derive electron density reflected upon the measured spectral profile.

The definition of hot component theory has to satisfy the equality of total metal abundances (Ca/Mg) and pressure of the radiant gas between the main and the hot components (Borovicka, 1993). However, the relation does not fit in most spectral data (e.g. Leonids). The Saha function is used to verify the definition but mostly finds negative values of electron density, which is clearly unrealistic (Kasuga et al., 2005b). This proves that the original hot component theory may go against its own definition (Borovicka, 1993). Kasuga et al. (2005b) suggest that the Ca II lines do not always belong to the hot component, but instead to the main component. Plausibility is also found in their low excitation energies (Ca II ≈ 3.1 eV), which are compatible with those of other neutral metals (e.g. Na I ≈ 2.1 eV) identified in the main component (Kasuga et al., 2007c). On the other hand, the hot component primarily consists of species with high excitation energies $\gtrsim$ 10 eV. Accordingly the Ca II lines are most likely to belong to the main component.

Given the difficulties in calculating absolute abundances, many researchers have employed simple line intensity ratios (e.g. Borovička et al., 2005). The method analyzes neutral atomic emission lines of Na I, Mg I, and (weak) Fe I only. Note that the intensity ratios do not directly reflect the elemental abundances due to no consideration for excitation properties of the elements and ions, including electron densities (e.g. Borovička, 2001; Borovička et al., 2005; Koten et al., 2006). Laboratory spectroscopic experiment proves that intensity ratios are not informative of the abundance and cannot be used to determine the meteorite analogue (Drouard et al., 2018). Line ratios can be used, at best, to study the trend of elemental content in meteors which happen to possess similar physical conditions (including similar entry velocities, similar strengths and similar excitation temperatures). Line intensity ratios can suggest the trend of elemental content in meteor showers but cannot provide the abundances.

8.6.3 Meteoroid Streams

Physical properties of meteoroids in meteoroid streams or debris in dust trails whose orbits do not intersect that of the Earth can be revealed by thermal and optical observations. The streams (or trails) and meteoroids mostly consist of mm to cm-scale compact aggregates, as estimated from the ratio of solar radiation pressure to solar gravity of $10^{-5} \lesssim \beta \lesssim 10^{-3}$ (e.g. Sykes and Walker, 1992; Reach et al., 2000, 2007; Ishiguro et al., 2002; Sarugaku et al., 2015).

Meteor ablation models in the Earth atmosphere are also available to estimate the size of meteoroids (Bronshten, 1983; Ceplecha et al., 1998). The classical models find typical meteors are 10μm – 10 cm in size, however, with uncertainties caused by various parameters (e.g. luminous efficiency, ablation coefficient, and fragmentation) which are sensitive to the meteoroid entry speed, tensile strength and brightness (Ceplecha et al., 1998; Babadzhanov, 2002). Faint meteors are estimated to be 10μm ~1 mm, but model improvements are needed to better represent fragmentation (Campbell-Brown and Koschny, 2004; Borovička et al., 2007).

8.6.4 Zodiacal Cloud

The zodiacal cloud is a circumsolar disk consisting of small dust particles supplied by comets and asteroids. The total mass is $\sim 4 \times 10^{16}$ kg, most (~90%?) of which is supplied by JFC disruptions and the rest by Oort cloud comets ($\lesssim$ 10%) and asteroids ($\lesssim$ 5%) (Nesvorný et al., 2010, 2011; Jenniskens, 2015). The supply rate needed to maintain the zodiacal cloud in steady-state is 10^3 to 10^4 kg s^{-1} (Nesvorný et al., 2011).

The fate of dust particles released from comets into the zodiacal cloud is traceable (cf. Grun et al., 1985). Sub-micron particles, with $\beta > 0.5$, are immediately blown out of the solar system on hyperbolic orbits by radiation pressure and are referred-to as β-meteoroids (Zook and Berg, 1975; Grun et al., 1985). The JFCs frequently disintegrate when near perihelion and form dust trails or meteoroid streams, mainly consisting of mm – cm sized dust particles (see section 8.6.3). The collisional lifetime of mm-scale particles at 1 AU is estimated to be $\tau_{\rm col} \gtrsim 10^5$ yr, modeled with the orbital distribution of sporadic meteors measured by radar (Nesvorný et al., 2011) (cf. $\tau_{\rm col} \sim 10^4$ or 10^5 yr, Grun et al., 1985; Soja et al., 2016; Yang and Ishiguro, 2018). On the other hand, Poynting-Robertson (P-R) and solar-wind drag cause dust particles to spiral down to the Sun. The P-R drag timescale, $\tau_{\rm PR}$, to drift down from $\bar{a} \sim 2.7$ AU with $\bar{e} \sim 0.8$ (objects with $T_J < 3.08$, see Table 8.1 and Figure 8.1) to 1 AU around the Earth orbit ($e \sim 0.017$) is calculated using the equation in Wyatt and Whipple (1950) (cf. Dermott et al., 2002),

$$\tau_{\rm PR} \simeq \frac{730}{\beta(1+sw)} \text{ yr}, \tag{8.9}$$

where $\beta \lesssim 10^{-3}$ (see 8.6.3) for dust particles of radius $\gtrsim$ 1 mm, with bulk density of 600 kg m^{-3} (Weissman et al., 2004), and $sw = 0.3$ is efficiency of solar-wind drag on a particle normalized to the P-R drag effect (Gustafson, 1994). The estimated P-R drag lifetime is $\tau_{\rm PR} \gtrsim 6{\times}10^5$ yr. This being somewhat longer than $\tau_{\rm col}$, the mm-scale dust particles are subject to collisional disruption while spiralling down to the Sun by P-R drag. As a result of competition between these two effects (loss to Poynting-Robertson at small sizes, loss to collisional shattering at large sizes), the 100–200μm dust particles are the most abundant in the zodiacal cloud (Love and Brownlee, 1993; Grun et al., 1985; Ceplecha et al., 1998; Nesvorný et al., 2010).

Nesvorný et al. (2011) noted that the collisional lifetime for mm-scale particles is long compared to the plausible lifetimes of most meteoroid streams ($\lesssim 10^4$ yr). They speculate that cm-scale particles are sources of smaller dust grains. Centimeter-scale particles are also released from JFCs. The sequence may result in a population of mm-sized or smaller particles which could be more resistant to collisions. Recent meteor observations suggest a relative lack of large particles (∼7 mm) (Jenniskens et al., 2016b), and also suggest that some of these larger particles disappear on timescales $\sim 10^4$ yr, not from collisions, but from other processes. Moorhead et al. (2017) finds a two-population sporadic meteoroid bulk density distribution suggesting that the physical character of freshly ejected dust particles could be altered over time. As another example, Rosetta dust collectors sampled both very pristine fluffy aggregates and compact particles ($\gtrsim 4$ cm in diameter) with a possible range of the dust bulk density from 400 to 3000 kg m^{-3} (Rotundi et al., 2015). This variety could have resulted from aggregate fragmentation into the denser collected grains as the spacecraft approached, while the packing effect is proposed as a plausible mechanism theory for fluffy dust particles released from comets (Mukai and Fechtig, 1983). The particle size could be reduced on a timescale of 10^4 –10^5 yr, comparable with the meteoroid stream lifetime. The effect makes the bulk density increase from 600 kg m^{-3} to 3000 kg m^{-3}, corresponding to shrinking the particle size approximately down to half. This could be a potential explanation for disappearing larger-scale dust particles in the meteoroid streams.

8.7 Summary and Future Work

In the last decade, a growing understanding of parent bodies and meteoroid streams has been achieved by combining new physical observations and dynamical investigations. Still, even where the associations are relatively clear, most complexes have multiple potential parent bodies and it remains unclear how the streams were formed.

Observationally, a major challenge is posed by the difficulty of measuring the physical characteristics of parent bodies, most of which are faint by virtue of their small size (typically $\lesssim$ a few km). They are also frequently observationally inaccessible because of their eccentric orbits, which cause them to spend most of the time far away near aphelion. Long-term surveillance of NEOs around their entire orbits might better reveal how and when parent bodies disintegrate and produce debris.

Dynamically, there are at least two challenging problems. One concerns the identification of parent bodies through the comparison of the orbital elements of meteoroids and potential parents by a D-criterion. Such methods work best for parents of young streams, where the effects of differential dynamical evolution are limited. However, in older systems, the dynamical elements have evolved enough to seriously undercut the use of the D-criteria. For this reason, for example, numerous Taurid parent bodies continue to be proposed. A key objective is to find a way to more reliably associate older meteoroid streams with their parent bodies. A second problem is the use of long-term dynamical simulations in which the initial conditions and/or potentially important non-gravitational effects are partly or wholly neglected.

We list key questions to be answered in the next decade.

1. Geminids: What process can act on ∼1000 yr timescales to produce the Geminid meteoroid stream? Phaethon appears dynamically associated with at least two kilometer-sized asteroids (2005 UD and 1999 YC) suggesting a past breakup or other catastrophe. But the likely timescale for such an event is ≫1000 yr. What caused the breakup and is it related to the Geminids? How many other PGC-related objects await discovery? Are Geminids represented in the meteorite collections and, if so, how can we identify them?
2. Quadrantids: Presumed parent 2003 EH_1 is currently inactive, but was recently as close to the Sun as is Phaethon at perihelion. Can residual mass loss in EH_1 be detected? Is the Quadrantid sodium abundance depleted as a result of the previously smaller perihelion? What physical difference is to be found in 96P which has a near-Sun orbit even now?
3. Capricornids: Several parent bodies have been proposed including both active comets and inactive asteroids. Did they originate from a common precursor? Is asteroid 2017 MB_1 related?
4. Taurids: The prime parent body is 2P/Encke but numerous additional parents with diverse properties continue to be proposed (mostly based on the D-criterion). How can we establish the relevance of these other objects to the Taurid stream? Can activity be detected? Is the D-criterion appropriate to judge?
5. Sekanina's (1973) Taurid-Perseids: Do 1566 Icarus and 2007 MK_6 share common physical properties? Is the sodium abundance in Taurid-Perseids depleted by solar heating due to the small perihelion?
6. Phoenicids, Andromedids and other minor complexes: Fragmentation is expected to produce a wide range of object sizes, with many bodies being too small to have been detected so far. What role can be played in the search for stream-related bodies by upcoming deep sky surveys, like the Large Synoptic Survey Telescope?
7. Which is the better index, the D-criterion (e.g. D_{SH}) or the dynamical invariants (C_1, C_2)?
8. How many near-Sun objects, driven by the Lidov-Kozai mechanism, exist?
9. What more can we learn from meteor spectroscopy, particularly of faint meteors?
10. Sporadic meteoroid populations tend to lose large dust particles (sizes $\gtrsim$ 7mm) on timescales of 10^4 yr. Why?

Acknowledgments

We are grateful to David Asher for his enthusiastic guidance to improve this chapter. TK thanks Takaya Okamoto for wholehearted assistance with this study and also Junichi Watanabe, Hideyo Kawakita, Mikiya Sato and Chie

Tsuchiya for support. We appreciate David Čapek, Jiří Borovička, Man-To Hui, Jing Li and Michael S. P. Kelley for figure contributions. We acknowledge reviews by Tadeusz Jopek and an anonymous reviewer. Lastly, we thank Galina Ryabova, again David Asher and Margaret Campbell-Brown for organizing this Meteoroids-book project.

REFERENCES

Abedin, A., Spurný, P., Wiegert, P. et al. 2015. On the age and formation mechanism of the core of the Quadrantid meteoroid stream. Icarus, **261**, 100–117.

Abedin, A., Wiegert, P., Pokorný, P., and Brown, P. 2017. The age and the probable parent body of the daytime arietid meteor shower. Icarus, **281**(Jan.), 417–443.

Abedin, A., Wiegert, P., Janches, D. et al. 2018. Formation and past evolution of the showers of 96P/Machholz complex. Icarus, **300**(Jan.), 360–385.

A'Hearn, M. F., Belton, M. J. S., Delamere, W. A. et al. 2005. Deep Impact: Excavating Comet Tempel 1. *Science*, **310**(Oct.), 258–264.

A'Hearn, Michael F., Millis, Robert C., Schleicher, David O., Osip, David J., and Birch, Peter V. 1995. The ensemble properties of comets: Results from narrowband photometry of 85 comets, 1976-1992. Icarus, **118**(Dec.), 223–270.

Anders, E., and Grevesse, N. 1989. Abundances of the elements - Meteoritic and solar. *Geochimica et Cosmochimica Acta*, **53**(Jan.), 197–214.

Angelis, G. De. 1995. Asteroid spin, pole and shape determinations. Planet. Space Sci., **43**(5), 649 – 682.

Ansdell, M., Meech, K. J., Hainaut, O. et al. 2014. Refined Rotational Period, Pole Solution, and Shape Model for (3200) Phaethon. ApJ, **793**(1), 50.

Antognini, J. M. O. 2015. Timescales of Kozai-Lidov oscillations at quadrupole and octupole order in the test particle limit. MNRAS, **452**(Oct.), 3610–3619.

Arendt, R. G. 2014. DIRBE Comet Trails. AJ, **148**(Dec.), 135.

Asher, D. J., and Clube, S. V. M. 1997. Towards a Dynamical History of 'Proto-Encke'. *Celestial Mechanics and Dynamical Astronomy*, **69**(Sept.), 149–170.

Asher, D. J., Clube, S. V. M., and Steel, D. I. 1993. Asteroids in the Taurid Complex. MNRAS, **264**(Sept.), 93.

Asher, D. J., Clube, S. V. M., Napier, W. M., and Steel, D. I. 1994. Coherent catastrophism. *Vistas in Astronomy*, **38**(Jan.), 1–27.

Baade, W., Cameron, R. C., and Folkman. 1950. 1949 MA = (1566) Icarus. *Minor Planet Circulars*, **347**(Jan.), 1.

Babadzhanov, P. B. 2001. Search for meteor showers associated with Near-Earth Asteroids. I. Taurid Complex. A&A, **373**(July), 329–335.

Babadzhanov, P. B. 2002. Fragmentation and densities of meteoroids. A&A, **384**(Mar.), 317–321.

Babadzhanov, P. B., and Obrubov, Y. V. 1987. Evolution of meteoroid streams. *Publications of the Astronomical Institute of the Czechoslovak Academy of Sciences*, **67**, 141–150.

Babadzhanov, P. B., and Obrubov, Y. V. 1991. P/Machholz 1986 VIII and Quadrantid Meteoroid Stream. Orbital Evolution and Interrelation. Page 8 of: *Asteroids, Comets, Meteors 1991*. LPI Contributions, vol. 765.

Babadzhanov, P. B., and Obrubov, Y. V. 1992a. Evolution of short-period meteoroid streams. *Celestial Mechanics and Dynamical Astronomy*, **54**(Mar.), 111–127.

Babadzhanov, P. B., and Obrubov, Y. V. 1992b (Sept.). P/Machholz 1986 8 and quadrantid meteoroid stream. Orbital evolution and relationship. In: Harris, A. W., and Bowell, E. (eds), *Asteroids, Comets, Meteors 1991*.

Babadzhanov, P. B., Williams, I. P., and Kokhirova, G. I. 2008. Meteor showers associated with 2003EH1. MNRAS, **386**(4), 2271–2277.

Babadzhanov, P. B., Williams, I. P., and Kokhirova, G. I. 2008. Near-Earth Objects in the Taurid complex. MNRAS, **386**(May), 1436–1442.

Bailey, M. E., Chambers, J. E., and Hahn, G. 1992. Origin of sungrazers - A frequent cometary end-state. *A & A*, **257**(Apr.), 315–322.

Beech, Martin. 2002. The age of the Geminids: a constraint from the spin-up time-scale. MNRAS, **336**(Oct.), 559–563.

Belton, M. J. S., Samarasinha, N. H., Fernández, Y. R., and Meech, K. J. 2005. The excited spin state of Comet 2P/Encke. Icarus, **175**(May), 181–193.

Blaauw, R. C. 2017. The mass index and mass of the Geminid meteoroid stream as determined with radar, optical and lunar impact data. Planet. Space Sci., **143**(Sept.), 83–88.

Borovicka, J. 1993. A fireball spectrum analysis. A&A, **279**(Nov.), 627–645.

Borovicka, J., and Weber, M. 1996. An alpha-Capricornid Meteor Spectrum. *WGN, Journal of the International Meteor Organization*, **24**(Apr.), 30–32.

Borovicka, J., Stork, R., and Bocek, J. 1999. First results from video spectroscopy of 1998 Leonid meteors. *Meteoritics and Planetary Science*, **34**(Nov.), 987–994.

Borovička, J., Koten, P., Spurný, P., Boček, J., and Štork, R. 2005. A survey of meteor spectra and orbits: evidence for three populations of Na-free meteoroids. Icarus, **174**(1), 15–30.

Borovička, J., Koten, P., Spurný, P. et al. 2009. Material properties of transition objects 3200 Phaethon and 2003 EH1. *Icy Bodies of the Solar System, Proceedings of the International Astronomical Union, IAU Symposium*, **5**(S263), 218–222.

Borovička, J. 2001 (Nov.). Video spectra of Leonids and other meteors. Pages 203–208 of: Warmbein, B. (ed), *Meteoroids 2001 Conference*. ESA Special Publication, vol. 495.

Borovička, J. 2007 (May). Properties of meteoroids from different classes of parent bodies. Pages 107–120 of: Valsecchi, G. B., Vokrouhlický, D., and Milani, A. (eds), *Near Earth Objects, our Celestial Neighbors: Opportunity and Risk*. IAU Symposium, vol. 236.

Borovička, J., Koten, P., Spurný, P. et al. 2010. Material properties of transition objects 3200 Phaethon and 2003 EH_1. Pages 218–222 of: Fernandez, J. A., Lazzaro, D., Prialnik,

D., and Schulz, R. (eds), *Icy Bodies of the Solar System*. IAU Symposium, vol. 263.

Borovička, J., Spurný, P., and Koten, P. 2007. Atmospheric deceleration and light curves of Draconid meteors and implications for the structure of cometary dust. A&A, **473**(Oct.), 661–672.

Borovička, J., Macke, R. J., Campbell-Brown, M. D. et al. 2019. Physical and Chemical Properties of Meteoroids. Chap. 2, pages **–** of: Ryabova, G. O., Asher, D. J., and Campbell-Brown, M. D. (eds), *Meteoroids: Sources of Meteors on the Earth and Beyond*. Cambridge, UK: Cambridge University Press.

Bottke, W. F., Jr., Nolan, M. C., Greenberg, R., and Kolvoord, R. A. 1994. Collisional Lifetimes and Impact Statistics of Near-earth Asteroids. Pages 337–357 of: Gehrels, T., Matthews, M. S., and Schumann, A. M. (eds), *Hazards Due to Comets and Asteroids*. University of Arizona Press, Tucson.

Britt, D. T., Yeomans, D., Housen, K., and Consolmagno, G. 2002. Asteroid Density, Porosity, and Structure. Pages 485–500 of: W. F. Bottke Jr., A. Cellino, P. Paolicchi, and Binzel, R. P. (eds), *Asteroids III*. University of Arizona Press, Tucson.

Bronshten, V. A. 1983. *Physics of meteoric phenomena*. Dordrecht, D. Reidel Publishing Co.

Brown, P., Weryk, R. J., Wong, D. K., and Jones, J. 2008a. A meteoroid stream survey using the Canadian Meteor Orbit Radar. I. Methodology and radiant catalogue. Icarus, **195**(May), 317–339.

Brown, P., Weryk, R. J., Wong, D. K., and Jones, J. 2008b. The Canadian Meteor Orbit Radar Meteor Stream Catalogue. *Earth Moon and Planets*, **102**(June), 209–219.

Brown, P., Wong, D. K., Weryk, R. J., and Wiegert, P. 2010. A meteoroid stream survey using the Canadian Meteor Orbit Radar. II: Identification of minor showers using a 3D wavelet transform. Icarus, **207**(May), 66–81.

Brown, P., Marchenko, V., Moser, D. E., Weryk, R., and Cooke, W. 2013. Meteorites from meteor showers: A case study of the Taurids. *Meteoritics and Planetary Science*, **48**(Feb.), 270–288.

Campbell-Brown, M. D., and Koschny, D. 2004. Model of the ablation of faint meteors. A&A, **418**(May), 751–758.

Campins, H., and Fernández, Y. 2002. Observational Constraints On Surface Characteristics Of Comet Nuclei. *Earth Moon and Planets*, **89**(Oct.), 117–134.

Čapek, D., and Borovička, J. 2009. Quantitative model of the release of sodium from meteoroids in the vicinity of the Sun: Application to Geminids. Icarus, **202**(2), 361–370.

Ceplecha, Z., Borovička, J., Elford, W. G. et al. 1998. Meteor Phenomena and Bodies. *Space Science Reviews*, **84**(Sept.), 327–471.

Chamberlin, A. B., McFadden, L.-A., Schulz, R., Schleicher, D. G., and Bus, S. J. 1996. 4015 Wilson-Harrington, 2201 Oljato, and 3200 Phaethon: Search for CN Emission. Icarus, **119**(Jan.), 173–181.

Chang, C.-K., Ip, W.-H., Lin, H.-W. et al. 2015. Asteroid Spin-rate Study Using the Intermediate Palomar Transient Factory. ApJS, **219**(Aug.), 27.

Chapman, C. R., Harris, A. W., and Binzel, R. 1994. Physical Properties of Near-earth Asteroids: Implications for the Hazard Issue. Page 537 of: Gehrels, T., Matthews, M. S., and Schumann, A. M. (eds), *Hazards Due to Comets and Asteroids*. University of Arizona Press, Tucson.

Clube, S. V. M., and Napier, W. M. 1984. The microstructure of terrestrial catastrophism. MNRAS, **211**(Dec.), 953–968.

Clube, S. V. M., and Napier, W. M. 1987. The cometary breakup hypothesis re-examined - A reply. MNRAS, **225**(Apr.), 55P–58P.

Cook, A. F. 1973. A Working List of Meteor Streams. *NASA Special Publication*, **319**, 183.

Dandy, C. L., Fitzsimmons, A., and Collander-Brown, S. J. 2003. Optical colors of 56 near-Earth objects: trends with size and orbit. Icarus, **163**(June), 363–373.

de León, J., Campins, H., Tsiganis, K., Morbidelli, A., and Licandro, J. 2010. Origin of the near-Earth asteroid Phaethon and the Geminids meteor shower. A&A, **513**(Apr.), A26.

DeMeo, F., and Binzel, R. P. 2008. Comets in the near-Earth object population. Icarus, **194**(Apr.), 436–449.

Dermott, S. F., Durda, D. D., Grogan, K., and Kehoe, T. J. J. 2002. Asteroidal Dust. Pages 423–442 of: Bottke, Jr., W. F., Cellino, A., Paolicchi, P., and Binzel, R. P. (eds), *Asteroids III*. University of Arizona Press, Tucson.

Drouard, A., Vernazza, P., Loehle, S. et al. 2018. Probing the use of spectroscopy to determine the meteoritic analogues of meteors. *A & A*, **613**(May), A54.

Duncan, M., Levison, H., and Dones, L. 2004. Dynamical evolution of ecliptic comets. Pages 193–204 of: M. C. Festou, H. U. Keller, and Weaver, H. A. (eds), *Comets II*. University of Arizona Press, Tucson.

Dundon, Luke R. 2005. *The enigmatic surface of (3200) Phaethon: Comparison with cometary candidates*. M.Phil. thesis, University of Hawaii at Manoa, Honolulu.

Emel'yanenko, V. V. 2017. Near-Sun asteroids. *Solar System Research*, **51**(Jan.), 59–63.

Fernández, J. A., Sosa, A., Gallardo, T., and Gutiérrez, J. N. 2014. Assessing the physical nature of near-Earth asteroids through their dynamical histories. Icarus, **238**(Aug.), 1–12.

Fernández, Y. R., Lisse, C. M., Ulrich Käufl, H. et al. 2000. Physical Properties of the Nucleus of Comet 2P/Encke. Icarus, **147**(Sept.), 145–160.

Foglia, S., Micheli, M., Ridley, H. B., Jenniskens, P., and Marsden, B. G. 2005. Comet D/1819 W1 (Blanpain) and 2003 WY25. *IAU Circ.*, **8485**(Feb.).

Gehrels, T., Roemer, E., Taylor, R. C., and Zellner, B. H. 1970. Minor planets and related objects. IV. Asteroid (1566) Icarus. AJ, **75**(Mar.), 186–195.

Gehrz, R. D., Reach, W. T., Woodward, C. E., and Kelley, M. S. 2006. Infrared observations of comets with the Spitzer Space Telescope. *Advances in Space Research*, **38**(Jan.), 2031–2038.

Gonczi, R., Rickman, H., and Froeschle, C. 1992. The connection between Comet P/Machholz and the Quadrantid meteor. MNRAS, **254**(Feb.), 627–634.

Green, D. W. E. 2005. Comets 169P/2002 EX_{12} (NEAT), 170P/2005 M1 (Christensen). *IAU Circ.*, **8591**(Aug.).

Green, S. F., Meadows, A. J., and Davies, J. K. 1985. Infrared observations of the extinct cometary candidate minor planet (3200) 1983TB. MNRAS, **214**(June), 29P–36P.

Grun, E., Zook, H. A., Fechtig, H., and Giese, R. H. 1985. Collisional balance of the meteoritic complex. Icarus, **62**(May), 244–272.

Gustafson, B. A. S. 1989. Geminid meteoroids traced to cometary activity on Phaethon. A&A, **225**(Nov.), 533–540.

Gustafson, B. A. S. 1994. Physics of Zodiacal Dust. *Annual Review of Earth and Planetary Sciences*, **22**, 553–595.

Hanuš, J., Delbo', M., Vokrouhlický, D. et al. 2016. Near-Earth asteroid (3200) Phaethon: Characterization of its orbit, spin

state, and thermophysical parameters. A&A, **592**(July), A34.

Harris, A. W. 1998. A Thermal Model for Near-Earth Asteroids. Icarus, **131**(Feb.), 291–301.

Harris, A. W., and Lagerros, J. S. V. 2002. Asteroids in the Thermal Infrared. Pages 205–218 of: Bottke, Jr., W. F., Cellino, A., Paolicchi, P., and Binzel, R. P. (eds), *Asteroids III*. University of Arizona Press, Tucson.

Harvey, G. A. 1973. Spectral Analysis of Four Meteors. *NASA Special Publication*, **319**, 103–129.

Hawkins, G. S., Southworth, R. B., and Steinon, F. 1959. Recovery of the Andromedids. AJ, **64**(June), 183.

Hicks, M. D., Fink, U., and Grundy, W. M. 1998. The Unusual Spectra of 15 Near-Earth Asteroids and Extinct Comet Candidates. Icarus, **133**(May), 69–78.

Hill, R. E., Gibbs, A. R., and Boattini, A. 2007. MPEC 2007-M32 : 2007 MK_6. *Minor Planet Electronic Circ.*, **2007-M32**.

Hirabayashi, M., Scheeres, D. J., Sánchez, D. P., and Gabriel, T. 2014. Constraints on the Physical Properties of Main Belt Comet P/2013 R3 from its Breakup Event. ApJ, **789**(July), L12.

Hoffmeister, C. 1937. *Die meteore, ihre kosmischen und irdischen beziehungen, von dr. C. Hoffmeister ... MIT 25 abbildungen im text und 4 tafeln.* Leipzig, Akademische verlagsgesellschaft m.b.h.

Holmberg, J., Flynn, C., and Portinari, L. 2006. The colours of the Sun. MNRAS, **367**(Apr.), 449–453.

Hsieh, H. H., and Jewitt, D. 2005. Search for Activity in 3200 Phaethon. ApJ, **624**(May), 1093–1096.

Hughes, D. W., and McBride, N. 1989. The mass of meteoroid streams. MNRAS, **240**(Sept.), 73–79.

Hui, M.-T. 2013. Observations of Comet P/2003 T12 = 2012 A3 (SOHO) at large phase angle in STEREO-B. MNRAS, **436**(Dec.), 1564–1575.

Hui, M.-T., and Li, J. 2017. Resurrection of (3200) Phaethon in 2016. AJ, **153**(Jan.), 23.

Huruhata, M., and Nakamura, J. 1957. Meteoric Shower Observed on December 5, 1956 in the Indian Ocean. *Tokyo Astronomical Bulletin., 2nd Ser.*, **99**, 1053–1054.

Ishiguro, M., Watanabe, J., Usui, F. et al. 2002. First Detection of an Optical Dust Trail along the Orbit of 22P/Kopff. ApJ, **572**(June), L117–L120.

Ishiguro, M., Sarugaku, Y., Nishihara, S. et al. 2009. Report on the Kiso cometary dust trail survey. *Advances in Space Research*, **43**(Mar.), 875–879.

Jakubík, M., and Neslušan, L. 2015. Meteor complex of asteroid 3200 Phaethon: its features derived from theory and updated meteor data bases. MNRAS, **453**(Oct.), 1186–1200.

Jenniskens, P. 1994. Meteor stream activity I. The annual streams. A&A, **287**(July), 990–1013.

Jenniskens, P. 2004. 2003 EH_1 Is the Quadrantid Shower Parent Comet. AJ, **127**(May), 3018–3022.

Jenniskens, P. 2006. *Meteor Showers and their Parent Comets*. Cambridge, UK: Cambridge University Press.

Jenniskens, P. 2008a. Meteoroid streams that trace to candidate dormant comets. Icarus, **194**(Mar.), 13–22.

Jenniskens, P. 2008b. Mostly Dormant Comets and their Disintegration into Meteoroid Streams: A Review. *Earth Moon and Planets*, **102**(June), 505–520.

Jenniskens, P. 2015. Meteoroid Streams and the Zodiacal Cloud. Pages 281–295 of: Michel, P., DeMeo, F. E., and Bottke, W. F. (eds), *Asteroids IV*. University of Arizona Press, Tucson.

Jenniskens, P. 2017. Meteor showers in review. Planet. Space Sci., **143**(Sept.), 116–124.

Jenniskens, P., and Lyytinen, E. 2005. Meteor Showers from the Debris of Broken Comets: D/1819 W_1 (Blanpain), 2003 WY_{25}, and the Phoenicids. AJ, **130**(Sept.), 1286–1290.

Jenniskens, P., and Nénon, Q. 2016. CAMS verification of single-linked high-threshold D-criterion detected meteor showers. Icarus, **266**(Mar.), 371–383.

Jenniskens, P., and Vaubaillon, J. 2007. 3D/Biela and the Andromedids: Fragmenting versus Sublimating Comets. AJ, **134**(Sept.), 1037–1045.

Jenniskens, P., and Vaubaillon, J. 2010. Minor Planet 2002 EX_{12} (=169P/NEAT) and the Alpha Capricornid Shower. AJ, **139**(May), 1822–1830.

Jenniskens, P., Nénon, Q., Gural, P. S. et al. 2016a. CAMS confirmation of previously reported meteor showers. Icarus, **266**(Mar.), 355–370.

Jenniskens, P., Nénon, Q., Gural, P. S. et al. 2016b. CAMS newly detected meteor showers and the sporadic background. Icarus, **266**(Mar.), 384–409.

Jewitt, D. 2004a. Looking through the HIPPO: Nucleus and Dust in Comet 2P/Encke. AJ, **128**(Dec.), 3061–3069.

Jewitt, D. 2006. Comet D/1819 W1 (Blanpain): Not Dead Yet. AJ, **131**(Apr.), 2327–2331.

Jewitt, D. 2012. The Active Asteroids. AJ, **143**(Mar.), 66.

Jewitt, D. 2013. Properties of Near-Sun Asteroids. AJ, **145**(May), 133.

Jewitt, D., and Hsieh, H. 2006. Physical Observations of 2005 UD: A Mini-Phaethon. AJ, **132**(Oct.), 1624–1629.

Jewitt, D., and Li, J. 2010. Activity in Geminid Parent (3200) Phaethon. AJ, **140**(Nov.), 1519–1527.

Jewitt, D., Li, J., and Agarwal, J. 2013. The Dust Tail of Asteroid (3200) Phaethon. ApJ, **771**(July), L36.

Jewitt, D., Agarwal, J., Li, J. et al. 2014. Disintegrating Asteroid P/2013 R3. ApJ, **784**(Mar.), L8.

Jewitt, D., Hsieh, H., and Agarwal, J. 2015. The Active Asteroids. Pages 221–241 of: Michel, P., DeMeo, F. E., and Bottke, W. F. (eds), *Asteroids IV*. University of Arizona Press.

Jewitt, D., Agarwal, J., Li, J. et al. 2017. Anatomy of an Asteroid Breakup: The Case of P/2013 R3. AJ, **153**(May), 223.

Jewitt, D. C. 2002. From Kuiper Belt Object to Cometary Nucleus: The Missing Ultrared Matter. AJ, **123**(Feb.), 1039–1049.

Jewitt, D. C. 2004b. From cradle to grave: the rise and demise of the comets. Pages 659–676 of: M. C. Festou, H. U. Keller, and Weaver, H. A. (eds), *Comets II*. University of Arizona Press, Tucson.

Jewitt, David, Mutchler, Max, Agarwal, Jessica, and Li, Jing. 2018. Hubble Space Telescope Observations of 3200 Phaethon at Closest Approach. AJ, **156**(Nov.), 238.

Jones, J. 1978. On the period of the Geminid meteor stream. MNRAS, **183**(May), 539–546.

Jones, J. 1986. The effect of gravitational perturbations on the evolution of the Taurid meteor stream complex. MNRAS, **221**(July), 257–267.

Jones, J., and Hawkes, R. L. 1986. The structure of the Geminid meteor stream. II - The combined action of the cometary ejection process and gravitational perturbations. MNRAS, **223**(Dec.), 479–486.

Jones, J., and Jones, W. 1993. Comet Machholz and the Quadrantid meteor stream. MNRAS, **261**(Apr.), 605–611.

Jopek, T. J. 2011. Meteoroid streams and their parent bodies. *Memorie della Societa Astronomica Italiana*, **82**, 310.

Jopek, T. J., and Jenniskens, P. M. 2011. The Working Group on Meteor Showers Nomenclature: A History, Current Status and a Call for Contributions. Pages 7–13 of: Cooke, W. J., Moser D. E. Hardin B. F., and Janches, D. (eds), *Meteoroids: The Smallest Solar System Bodies*. Colorado, USA: Proceedings of the Meteoroids Conference held in Breckenridge, NASA/CP-2011-216469.

Kańuchová, Z., and Neslušan, L. 2007. The parent bodies of the Quadrantid meteoroid stream. A&A, **470**(Aug.), 1123–1136.

Kasuga, T., and Jewitt, D. 2008. Observations of 1999 YC and the Breakup of the Geminid Stream Parent. AJ, **136**(Aug.), 881–889.

Kasuga, T., and Jewitt, D. 2015. Physical Observations of (196256) 2003 EH1, Presumed Parent of the Quadrantid Meteoroid Stream. AJ, **150**(Nov.), 152.

Kasuga, T., Watanabe, J., and Ebizuka, N. 2005a. A 2004 Geminid meteor spectrum in the visible-ultraviolet region. Extreme Na depletion? A&A, **438**(Aug.), L17–L20.

Kasuga, T., Yamamoto, T., Watanabe, J. et al. 2005b. Metallic abundances of the 2002 Leonid meteor deduced from high-definition TV spectra. A&A, **435**(May), 341–351.

Kasuga, T., Watanabe, J.-I., and Sato, M. 2006. Benefits of an impact mission to 3200 Phaethon: nature of the extinct comet and artificial meteor shower. MNRAS, **373**(Dec.), 1107–1111.

Kasuga, T., Yamamoto, T., Kimura, H., and Watanabe, J. 2006. Thermal desorption of Na in meteoroids. A&A, **453**(2), L17–L20.

Kasuga, T., Sato, M., and Watanabe, J. 2007a. Creating an artificial Geminid meteor shower: Correlation between ejecta velocity and observability. *Advances in Space Research*, **40**, 215–219.

Kasuga, T., Iijima, T., and Watanabe, J. 2007b. Is a 2004 Leonid meteor spectrum captured in a 182 cm telescope? A&A, **474**(Nov.), 639–645.

Kasuga, T., Watanabe, J., Kawakita, H., and Yamamoto, T. 2007c. The origin of the Ca(II) emission, in one of two plasma components, and the metallic abundances in a 2002 Leonid meteor spectrum. *Advances in Space Research*, **39**, 513–516.

Kasuga, T., Balam, D. D., and Wiegert, P. A. 2010. Comet 169P/NEAT(=2002 EX_{12}): The Parent Body of the α-Capricornid Meteoroid Stream. AJ, **140**(Dec.), 1806–1813.

Kelley, Michael S., Woodward, Charles E., Harker, David E. et al. 2006. A Spitzer Study of Comets 2P/Encke, 67P/Churyumov-Gerasimenko, and C/2001 HT50 (LINEAR-NEAT). ApJ, **651**(Nov.), 1256–1271.

Killen, R. M., Sarantos, M., Potter, A. E., and Reiff, P. 2004. Source rates and ion recycling rates for Na and K in Mercury's atmosphere. Icarus, **171**(Sept.), 1–19.

Kinoshita, D., Ohtsuka, K., Sekiguchi, T. et al. 2007. Surface heterogeneity of 2005 UD from photometric observations. A&A, **466**(May), 1153–1158.

Kokotanekova, R., Snodgrass, C., Lacerda, P. et al. 2017. Rotation of cometary nuclei: new light curves and an update of the ensemble properties of Jupiter-family comets. MNRAS, **471**(Nov.), 2974–3007.

Kondrat'eva, E. D., Murav'eva, I. N., and Reznikov, E. D. 1997. On the Forthcoming Return of the Leonid Meteoric Swarm. *Solar System Research*, **31**, 489.

Kosai, H. 1992. Short-period comets and Apollo-Amor-Aten type asteroids in view of Tisserand invariant. *Celestial Mechanics and Dynamical Astronomy*, **54**(Mar.), 237–240.

Koten, P., Borovička, J., Spurný, P. et al. 2006. Double station and spectroscopic observations of the Quadrantid meteor shower and the implications for its parent body. MNRAS, **366**(Mar.), 1367–1372.

Kozai, Y. 1962. Secular perturbations of asteroids with high inclination and eccentricity. AJ, **67**(Nov.), 591.

Kresak, L. 1982. On the similarity of orbits of associated comets, asteroids and meteoroids. *Bulletin of the Astronomical Institutes of Czechoslovakia*, **33**(May), 104–110.

Kronk, G. W. 1988. *Meteor showers. A descriptive catalog*. Hillside, N.J.: Enslow Publishersm.

Kronk, G. W. 1999. *Cometography: A Catalog of Comets, Volume 1: Ancient-1799*. UK: Cambridge University Press.

Lamy, P. L., Toth, I., Fernandez, Y. R., and Weaver, H. A. 2004. The sizes, shapes, albedos, and colors of cometary nuclei. Pages 223–264 of: Festou, M. C., Keller, H. U., and Weaver, H. A. (eds), *Comets II*. Tucson: University of Arizona Press.

Lauriello, P.J. 1974. Application of a convective heat source to the thermal fracturing of rock. *International Journal of Rock Mechanics and Mining Sciences & Geomechanics Abstracts*, **11**(2), 75 – 81.

Levison, H. F. 1996. Comet Taxonomy. Pages 173–191 of: Rettig, T., and Hahn, J. M. (eds), *Completing the Inventory of the Solar System*. Astronomical Society of the Pacific Conference Series, vol. 107.

Levison, H. F., Terrell, D., Wiegert, P. A., Dones, L., and Duncan, M. J. 2006. On the origin of the unusual orbit of Comet 2P/Encke. Icarus, **182**(May), 161–168.

Li, J., and Jewitt, D. 2013. Recurrent Perihelion Activity in (3200) Phaethon. AJ, **145**(June), 154.

Licandro, J., Tancredi, G., Lindgren, M., Rickman, H., and Hutton, R. G. 2000. CCD Photometry of Cometary Nuclei, I: Observations from 1990-1995. Icarus, **147**(Sept.), 161–179.

Licandro, J., Campins, H., Mothé-Diniz, T., Pinilla-Alonso, N., and de León, J. 2007. The nature of comet-asteroid transition object (3200) Phaethon. *A & A*, **461**(Jan.), 751–757.

Lidov, M. L. 1962. The evolution of orbits of artificial satellites of planets under the action of gravitational perturbations of external bodies. Planet. Space Sci., **9**(Oct.), 719–759.

Lindblad, B. A. 1987. Physics and Orbits of Meteoroids. Page 229 of: Fulchignoni, M., and Kresak, L. (eds), *The Evolution of the Small Bodies of the Solar System*.

Lisse, C. M., Fernández, Y. R., A'Hearn, M. F. et al. 2004. A tale of two very different comets: ISO and MSX measurements of dust emission from 126P/IRAS (1996) and 2P/Encke (1997). Icarus, **171**(Oct.), 444–462.

Lodders, K. 2003. Solar System Abundances and Condensation Temperatures of the Elements. ApJ, **591**(July), 1220–1247.

Love, S. G., and Brownlee, D. E. 1993. A Direct Measurement of the Terrestrial Mass Accretion Rate of Cosmic Dust. *Science*, **262**(5133), 550–553.

Lowry, S. C., and Weissman, P. R. 2007a. Rotation and color properties of the nucleus of Comet 2P/Encke. Icarus, **188**(1), 212–223.

Lowry, Stephen C., and Weissman, Paul R. 2007b. Rotation and color properties of the nucleus of Comet 2P/Encke. *Icarus*, **188**(1), 212 – 223.

Madiedo, J. M., Trigo-Rodríguez, J. M., Ortiz, J. L., Castro-Tirado, A. J., and Cabrera-Caño, J. 2014. Orbit and emission spectroscopy of α-Capricornid fireballs. Icarus, **239**(Sept.), 273–280.

Mahapatra, P. R., Ostro, Steven J., Benner, L. A. m. et al. 1999. Recent radar observations of asteroid 1566 Icarus. *Planetary and Space Science*, **47**(Aug.), 987–995.

Mainzer, A., Grav, T., Bauer, J. et al. 2011. NEOWISE Observations of Near-Earth Objects: Preliminary Results. ApJ, **743**(Dec.), 156.

Matlovič, P., Tóth, J., Rudawska, R., and Kornoš, L. 2017. Spectra and physical properties of Taurid meteoroids. Planet. Space Sci., **143**(Sept.), 104–115.

McGrath, M. A., Johnson, R. E., and Lanzerotti, L. J. 1986. Sputtering of sodium on the planet Mercury. Nature, **323**(Oct.), 694–696.

McIntosh, B. A. 1990. Comet P/Machholtz and the Quadrantid meteor stream. Icarus, **86**(July), 299–304.

McNaught, R. H., and Asher, D. J. 1999. Leonid Dust Trails and Meteor Storms. *WGN, Journal of the International Meteor Organization*, **27**(Apr.), 85–102.

Meech, K. J., Hainaut, O. R., and Marsden, B. G. 2004. Comet nucleus size distributions from HST and Keck telescopes. Icarus, **170**(Aug.), 463–491.

Micheli, M. 2005. Possibile correlazione tra l'asteroide 2003 WY_{25}, la cometa D/1819 W1 (Blanpain) e due sciami meteorici occasionali. *Astronomia. La rivista dell' Unione Astrofili Italiani*, **1**(Feb.), 47–53.

Millman, P. M. 1955. Meteor News- Photographic Meteor Spectra (Appendix 3); Orionid and Geminid Observations at Montreal; A Provisional Supplementary List of Meteor Showers. JRASC, **49**(Aug.), 169.

Millman, P. M. 1980. One hundred and fifteen years of meteor spectroscopy. Pages 121–127 of: Halliday, I., and McIntosh, B. A. (eds), *Solid Particles in the Solar System*. IAU Symposium, vol. 90. Dordrecht, D. Reidel Publishing Co.

Millman, P. M., and McKinley, D. W. R. 1963. Meteors. Pages 674–773 of: Kuiper, G. P., and Middlehurst, B. M. (eds), *The Moon Meteorites and Comets*. The University of Chicago Press.

Miner, E., and Young, J. 1969. Photometric Determination of the Rotation Period of 1566 Icarus. Icarus, **10**(May), 436–440.

Moiseev, N. D. 1945. On Certain Basic Simplified Schemes of Celestial Mechanics Obtained With the Aid of Averaging Different Variants of the Problem of Three Bodies (in Russian). *Trudy Gosudarstvennogo astronomicheskogo instituta im Sternberga*, **15**, 75–99.

Molaro, Jamie L., Byrne, Shane, and Langer, Stephen A. 2015. Grain-scale thermoelastic stresses and spatiotemporal temperature gradients on airless bodies, implications for rock breakdown. *Journal of Geophysical Research (Planets)*, **120**(Feb.), 255–277.

Moorhead, A. V., Blaauw, R. C., Moser, D. E. et al. 2017. A two-population sporadic meteoroid bulk density distribution and its implications for environment models. MNRAS, **472**(Dec.), 3833–3841.

Mukai, T., and Fechtig, H. 1983. Packing effect of fluffy particles. Planet. Space Sci., **31**(June), 655–658.

Musci, R., Weryk, R. J., Brown, P., Campbell-Brown, M. D., and Wiegert, P. A. 2012. An Optical Survey for Millimeter-sized Interstellar Meteoroids. ApJ, **745**(Feb.), 161.

Nagasawa, K. 1978. Analysis of the spectra of Leonid meteors. *Annals of the Tokyo Astronomical Observatory*, **16**, 157–187.

Neslušan, L., Hajduková, M., and Jakubík, M. 2013a. Meteor-shower complex of asteroid 2003 EH1 compared with that of comet 96P/Machholz. A&A, **560**(Dec.), A47.

Neslušan, L., Kaňuchová, Z., and Tomko, D. 2013b. The meteor-shower complex of 96P/Machholz revisited. A&A, **551**(Mar.), A87.

Neslušan, L., Kaňuchová, Z., and Tomko, D. 2014. The ecliptic-toroidal structure of the meteor complex of comet 96P/Machholz. Pages 235–242 of: Jopek, T. J., Rietmeijer, F. J. M., Watanabe, J., and Williams, I. P. (eds), *Proc. International Conf. held at A.M. University in Poznań, Poland, August 26-30, 2013. Meteoroids 2013*. Poznań: Wydanictwo Naukowe UAM.

Nesvorný, D., Jenniskens, P., Levison, H. F. et al. 2010. Cometary Origin of the Zodiacal Cloud and Carbonaceous Micrometeorites. Implications for Hot Debris Disks. ApJ, **713**(Apr.), 816–836.

Nesvorný, D., Janches, D., Vokrouhlický, D. et al. 2011. Dynamical Model for the Zodiacal Cloud and Sporadic Meteors. ApJ, **743**(Dec.), 129.

Nugent, C. R., Mainzer, A., Masiero, J. et al. 2015. NEOWISE Reactivation Mission Year One: Preliminary Asteroid Diameters and Albedos. ApJ, **814**(Dec.), 117.

Ohtsuka, K., Yoshikawa, M., and Watanabe, J.-I. 1995. Impulse Effects on the Orbit of 1987 Quadrantid Swarm. PASJ, **47**(Aug.), 477–486.

Ohtsuka, K., Sekiguchi, T., Kinoshita, D. et al. 2006. Apollo asteroid 2005 UD: split nucleus of (3200) Phaethon? A&A, **450**(May), L25–L28.

Ohtsuka, K., Arakida, H., Ito, T. et al. 2007. Apollo Asteroids 1566 Icarus and 2007 MK_6: Icarus Family Members ? ApJ, **668**(Oct.), L71–L74.

Ohtsuka, K., Arakida, H., Ito, T., Yoshikawa, M., and Asher, D. J. 2008a. Apollo Asteroid 1999 YC: Another Large Member of the PGC? *Meteoritics and Planetary Science Supplement*, **43**(Aug.), 5055.

Ohtsuka, K., Yoshikawa, M., Watanabe, J. et al. 2008b. On the Substantial Spatial Spread of the Quadrantid Meteoroid Stream. *Earth Moon and Planets*, **102**(June), 179–182.

Ohtsuka, K., Nakato, A., Nakamura, T. et al. 2009. Solar-Radiation Heating Effects on 3200 Phaethon. PASJ, **61**(Dec.), 1375–1387.

Ohtsuka, Katsuhito, Shimoda, Chikara, Yoshikawa, Makoto, and Watanabe, Jun-Ichi. 1997. Activity Profile of the Sextantid Meteor Shower. *Earth Moon and Planets*, **77**(Apr.), 83–91.

Olech, A., Żołądek, P., Wiśniewski, M. et al. 2017. Enhanced activity of the Southern Taurids in 2005 and 2015. MNRAS, **469**(Aug.), 2077–2088.

Olivier, C. P. 1925. *Meteors*. Baltimore, Williams & Wilkins company.

Olmsted, D. 1834. Observations of the meteors of November 13, 1833. *American Journal of Science*, **25**, 354–411.

Ortiz, J. L., Madiedo, J. M., Morales, N., Santos-Sanz, P., and Aceituno, F. J. 2015. Lunar impact flashes from Geminids: analysis of luminous efficiencies and the flux of large meteoroids on Earth. MNRAS, **454**(Nov.), 344–352.

Pariseau, G. William. 2006. *Design Analysis in Rock Mechanics*. London: Taylor and Francis.

Popescu, M., Birlan, M., Nedelcu, D. A., Vaubaillon, J., and Cristescu, C. P. 2014. Spectral properties of the largest asteroids associated with Taurid Complex. A&A, **572**(Dec.), A106.

Porubčan, V., Williams, I. P., and Kornoš, L. 2004. Associations Between Asteroids and Meteoroid Streams. *Earth Moon and Planets*, **95**(Dec.), 697–712.

Porubčan, V., Kornoš, L., and Williams, I. P. 2006. The Taurid complex meteor showers and asteroids. *Contributions of the Astronomical Observatory Skalnate Pleso*, **36**(June), 103–117.

Potter, A. E., Killen, R. M., and Morgan, T. H. 2000. Variation of lunar sodium during passage of the Moon through the Earth's magnetotail. *Journal of Geophysical Research*, **105**(June), 15073–15084.

Pravec, P., Harris, A. W., Vokrouhlický, D. et al. 2008. Spin rate distribution of small asteroids. Icarus, **197**(Oct.), 497–504.

Quetelet, Lambert Adolphe Jacques. 1839. *Catalogue des principles apparitions d'etoiles filantes*. Bruxelles, M. Hayez, imprimeur, 1839.

Reach, W. T., Sykes, M. V., Lien, D., and Davies, J. K. 2000. The Formation of Encke Meteoroids and Dust Trail. Icarus, **148**(Nov.), 80–94.

Reach, W. T., Kelley, M. S., and Sykes, M. V. 2007. A survey of debris trails from short-period comets. Icarus, **191**(Nov.), 298–322.

Richter, Dorothy, and Simmons, Gene. 1974. Thermal expansion behavior of igneous rocks. *International Journal of Rock Mechanics and Mining Sciences & Geomechanics Abstracts*, **11**(10), 403 – 411.

Ridley, H. B. 1957. *Circ. British Astron. Assoc.*, **382**.

Ridley, H. B. 1963. The Phoenicid Meteor Shower of 1956 December 5. *Monthly Notes of the Astronomical Society of South Africa*, **22**(Jan.), 42.

Rotundi, A., Sierks, H., Della Corte, V. et al. 2015. Dust measurements in the coma of comet 67P/Churyumov-Gerasimenko inbound to the Sun. *Science*, **347**(1), aaa3905.

Rozitis, B., and Green, S. F. 2013. The strength and detectability of the YORP effect in near-Earth asteroids: a statistical approach. MNRAS, **430**(Apr.), 1376–1389.

Rudawska, R., Matlovič, P., Tóth, J., and Kornoš, L. 2015. Independent identification of meteor showers in EDMOND database. Planet. Space Sci., **118**(Dec.), 38–47.

Russell, J. A., Sadoski, Jr., M. J., Sadoski, D. C., and Wetzel, G. F. 1956. The Spectrum of a Geminid Meteor. *Publications of the Astronomical Society of the Pacific*, **68**(Feb.), 64.

Ryabova, G. O. 1999. Age of the Geminid Meteor Stream (Review). *Solar System Research*, **33**(Jan.), 224–238.

Ryabova, G. O. 2017. The mass of the Geminid meteoroid stream. *Planetary and Space Science*, **143**(Sept.), 125–131.

Sarli, Bruno Victorino, Horikawa, Makoto, Yam, Chit Hong, Kawakatsu, Yasuhiro, and Yamamoto, Takayuki. 2018. DESTINY+ Trajectory Design to (3200) Phaethon. *Journal of the Astronautical Sciences*, **65**(Mar.), 82–110.

Sarugaku, Y., Ishiguro, M., Ueno, M., Usui, F., and Reach, W. T. 2015. Infrared and Optical Imagings of the Comet 2P/Encke Dust Cloud in the 2003 Return. ApJ, **804**(May), 127.

Sasaki, S., Nakamura, K., Hamabe, Y., Kurahashi, E., and Hiroi, T. 2001. Production of iron nanoparticles by laser irradiation in a simulation of lunar-like space weathering. Nature, **410**(Mar.), 555–557.

Sato, M., Watanabe, J.-i., Tsuchiya, C. et al. 2017. Detection of the Phoenicids meteor shower in 2014. Planet. Space Sci., **143**(Sept.), 132–137.

Scheeres, D. J., Hartzell, C. M., Sánchez, P., and Swift, M. 2010. Scaling forces to asteroid surfaces: The role of cohesion. Icarus, **210**(Dec.), 968–984.

Scheeres, Daniel J., and Sánchez, Paul. 2018. Implications of cohesive strength in asteroid interiors and surfaces and its measurement. *Progress in Earth and Planetary Science*, **5**(Dec.), 25.

Sekanina, Z. 1973. Statistical Model of Meteor Streams. III. Stream Search Among 19303 Radio Meteors. Icarus, **18**(Feb.), 253–284.

Sekanina, Z., and Chodas, P. W. 2005. Origin of the Marsden and Kracht Groups of Sunskirting Comets. I. Association with Comet 96P/Machholz and Its Interplanetary Complex. ApJS, **161**(2), 551.

Skiff, B. A. 2003. MPEC 2003-E27: 2003 EH_1. *Minor Planet Electronic Circ.*, **2003-E27**.

Soja, R. H., Schwarzkopf, G. J., Sommer, M. et al. 2016 (Jan.). Collisional lifetimes of meteoroids. Page 284 of: *International Meteor Conference Egmond, the Netherlands, 2-5 June 2016*.

Sosa, A., and Fernández, J. A. 2015. Comets 169P/NEAT and P/2003 T12 (SOHO): Two possible fragments of a common ancestor? *IAU General Assembly*, **22**(Aug.), 2255583.

Southworth, R. B., and Hawkins, G. S. 1963. Statistics of meteor streams. *Smithsonian Contributions to Astrophysics*, **7**, 261–285.

Springmann, Alessondra, Lauretta, Dante S., Klaue, Bjoern et al. 2018. Thermal Alteration of Labile Elements in Carbonaceous Chondrites. *Icarus*, in press, available online 2018 December 10.

Spurný, P. 1993. Geminids from photographic records. Page 193 of: Stohl, J., and Williams, I. P. (eds), *Meteoroids and their Parent Bodies*.

Spurný, P., Borovička, J., Mucke, H., and Svoreň, J. 2017. Discovery of a new branch of the Taurid meteoroid stream as a real source of potentially hazardous bodies. A&A, **605**(Sept.), A68.

Steel, D. I., and Asher, D. J. 1996. The orbital dispersion of the macroscopic Taurid objects. MNRAS, **280**(June), 806–822.

Suggs, R. M., Moser, D. E., Cooke, W. J., and Suggs, R. J. 2014. The flux of kilogram-sized meteoroids from lunar impact monitoring. Icarus, **238**(Aug.), 23–36.

Sykes, M. V., and Walker, R. G. 1992. Cometary dust trails. I - Survey. Icarus, **95**(Feb.), 180–210.

Szalay, Jamey R., Pokorný, Petr, Jenniskens, Peter, and Horányi, Mihály. 2018. Activity of the 2013 Geminid meteoroid stream at the Moon. MNRAS, **474**(Mar.), 4225–4231.

Tancredi, G. 2014. A criterion to classify asteroids and comets based on the orbital parameters. Icarus, **234**(May), 66–80.

Taylor, P. A., Marshall, S. E., Venditti, F. et al. 2018 (Mar.). Radar and Infrared Observations of Near-Earth Asteroid 3200 Phaethon. Page 2509 of: *Lunar and Planetary Science Conference*.

Tedesco, E. F., Noah, P. V., Noah, M., and Price, S. D. 2004. IRAS Minor Planet Survey V6.0. *NASA Planetary Data System*, Oct., IRAS.

Tholen, D. J. 1984 (Sept.). *Asteroid taxonomy from cluster analysis of photometry*. Ph.D. thesis, University of Arizona, Tucson.

Ticha, J., Tichy, M., Kocer, M. et al. 2003. 2003 WY_{25}. *Minor Planet Electronic Circulars*, **2003-W41**(Nov.).

Todorović, Nataša. 2018. The dynamical connection between Phaethon and Pallas. MNRAS, **475**(Mar.), 601–604.

Trigo-Rodríguez, J. M., Llorca, J., Borovicka, J., and Fabregat, J. 2003. Chemical abundances determined from meteor spectra: I Ratios of the main chemical elements. *Meteoritics and Planetary Science*, **38**(Aug.), 1283–1294.

Trigo-Rodríguez, J. M., Llorca, J., and Fabregat, J. 2004. Chemical abundances determined from meteor spectra - II. Evidence for enlarged sodium abundances in meteoroids. MNRAS, **348**(Mar.), 802–810.

Tsuchiya, C., Sato, M., Watanabe, J.-i. et al. 2017. Correction effect to the dispersion of radiant point in case of low velocity meteor showers. Planet. Space Sci., **143**(Sept.), 142–146.

Tubiana, C., Snodgrass, C., Michelsen, R. et al. 2015. 2P/Encke, the Taurid complex NEOs and the Maribo and Sutter's Mill meteorites. A&A, **584**(Dec.), A97.

Vaubaillon, J., Arlt, R., Shanov, S., Dubrovski, S., and Sato, M. 2005. The 2004 June Bootid meteor shower. MNRAS, **362**(Oct.), 1463–1471.

Vaubaillon, J., Neslušan, L., Sekhar, A., Rudawska, R., and Ryabova, G. 2019. From Parent Body to Meteor Shower: the Dynamics of Meteoroid Streams. Chap. 7, pages **–** of: Ryabova, G. O., Asher, D. J., and Campbell-Brown, M. D. (eds), *Meteoroids: Sources of Meteors on the Earth and Beyond*. Cambridge, UK: Cambridge University Press.

Veeder, G. J., Hanner, M. S., Matson, D. L. et al. 1989. Radiometry of near-earth asteroids. AJ, **97**(Apr.), 1211–1219.

Vokrouhlický, D., Bottke, W. F., Chesley, S. R., Scheeres, D. J., and Statler, T. S. 2015. The Yarkovsky and YORP Effects. Pages 509–531 of: Patrick Michel, Francesca E. DeMeo, and Bottke, William F. (eds), *Asteroids IV*. University of Arizona Press, Tucson.

Voloshchuk, I. I., and Kashcheev, B. L. 1986. Study of the structure of a meteor complex near the earth's orbit. I - Description of the model. *Solar System Research / Translation. Astronomicheskii Vestnik*, **19**(Apr.), 213–216.

Warner, B. D. 2017. Near-Earth Asteroid Lightcurve Analysis at CS3-Palmer Divide Station: 2016 October-December. *Minor Planet Bulletin*, **44**(Apr.), 98–107.

Warner, B. D., and Fitzsimmons, A. 2005. Comet P/2002 EX_12 (NEAT). *IAU Circ.*, **8578**(Aug.).

Warner, Brian D. 2018. Near-Earth Asteroid Lightcurve Analysis at CS3-Palmer Divide Station: 2017 July Through October. *Minor Planet Bulletin*, **45**(Jan.), 19–34.

Warner, Brian D., Harris, Alan W., and Pravec, Petr. 2009. The asteroid lightcurve database. *Icarus*, **202**(1), 134 – 146.

Watanabe, J.-I., Sato, M., and Kasuga, T. 2005. Phoenicids in 1956 Revisited. PASJ, **57**(Oct.), L45–L49.

Weissman, P. R., Asphaug, E., and Lowry, S. C. 2004. Structure and density of cometary nuclei. Pages 337–357 of: M. C. Festou, H. U. Keller, and Weaver, H. A. (eds), *Comets II*. University of Arizona Press, Tucson.

Weryk, Robert J., and Brown, Peter G. 2012. Simultaneous radar and video meteors—I: Metric comparisons. Planet. Space Sci., **62**(Mar.), 132–152.

Whipple, F. L. 1939a. Photographic meteor studies I. Page 136 of: *Publications of the American Astronomical Society*. Publications of the American Astronomical Society, vol. 9.

Whipple, F. L. 1939b. Photographic study of the Geminid meteor shower. Page 274 of: *Publications of the American Astronomical Society*. Publications of the American Astronomical Society, vol. 9.

Whipple, F. L. 1983. 1983 TB and the Geminid Meteors. *IAU Circ.*, **3881**(Oct.).

Whipple, Fred. L. 1940. Photographic Meteor Studies. III. The Taurid Shower. *Proceedings of the American Philosophical Society*, **83**(Oct.), 711–745.

Wiegert, P., and Brown, P. 2004. The problem of linking minor meteor showers to their parent bodies: initial considerations. *Earth Moon and Planets*, **95**(Dec.), 19–26.

Wiegert, P., and Brown, P. 2005. The Quadrantid meteoroid complex. Icarus, **179**(Dec.), 139–157.

Wiegert, P., Clark, D., Campbell-Brown, M., and Brown, P. 2017. Minor Planet 2017 MB_1 and the Alpha Capricornids Meteor Shower. *Central Bureau Electronic Telegrams*, **4415**(Aug.).

Wiegert, P. A., Houde, M., and Peng, R. 2008. An upper limit on gas production from 3200 Phaethon. Icarus, **194**(Apr.), 843–846.

Wiegert, P. A., Brown, P. G., Weryk, R. J., and Wong, D. K. 2013. The Return of the Andromedids Meteor Shower. AJ, **145**(Mar.), 70.

Wilkison, Sarah L., and Robinson, Mark S. 2000. Bulk density of ordinary chondrite meteorites and implications for asteroidal internal structure. *Meteoritics and Planetary Science*, **35**(Nov.), 1203–1213.

Williams, I. P., and Wu, Z. 1993. The Geminid meteor stream and asteroid 3200 Phaethon. MNRAS, **262**(May), 231–248.

Williams, I. P., Ryabova, G. O., Baturin, A. P., and Chernitsov, A. M. 2004. The parent of the Quadrantid meteoroid stream and asteroid 2003 EH1. MNRAS, **355**(Dec.), 1171–1181.

Williams, I. P., Jopek, T. J., Rudawska, R., Tóth, J., and Kornoš, L. 2019. Minor Meteor Showers and the Sporadic Background. Chap. 9, pages **–** of: Ryabova, G. O., Asher, D. J., and Campbell-Brown, M. D. (eds), *Meteoroids: Sources of Meteors on the Earth and Beyond*. Cambridge, UK: Cambridge University Press.

Wyatt, S. P., and Whipple, F. L. 1950. The Poynting-Robertson effect on meteor orbits. ApJ, **111**(Jan.), 134–141.

Yakshinskiy, B. V., and Madey, T. E. 2004. Photon-stimulated desorption of Na from a lunar sample: temperature-dependent effects. Icarus, **168**(Mar.), 53–59.

Yamamoto, T. 1985. Formation environment of cometary nuclei in the primordial solar nebula. A&A, **142**(Jan.), 31–36.

Yanagisawa, M., Ikegami, H., Ishida, M. et al. 2008. Lunar Impact Flashes by Geminid Meteoroids in 2007. *Meteoritics and Planetary Science Supplement*, **43**(Aug.), 5169.

Yang, H., and Ishiguro, M. 2018. Evolution of Cometary Dust Particles to the Orbit of the Earth: Particle Size, Shape, and Mutual Collisions. ApJ, **854**(Feb.), 173.

Ye, Q.-Z., Brown, P. G., and Pokorný, P. 2016. Dormant comets among the near-Earth object population: a meteor-based survey. MNRAS, **462**(Nov.), 3511–3527.

Ye, Quan-Zhi. 2018. Meteor showers from active asteroids and dormant comets in near-Earth space: A review. Planet. Space Sci., 1–6.

Zook, H. A., and Berg, O. E. 1975. A source for hyperbolic cosmic dust particles. Planet. Space Sci., **23**(Jan.), 183–203.